Rainflow-counting matrix interpolation over different operating conditions for hydroelectric turbine fatigue assessment

Quang Hung Pham, Martin Gagnon, Jérôme Antoni, Antoine Tahan, Christine Monette

Version of Record: https://www.sciencedirect.com/science/article/pii/S0960148121003906
Manuscript_63f2254949b93f1d19ed8cb36bc78bb7

Rainflow-counting matrix interpolation over different operating conditions for hydroelectric turbine fatigue assessment

Quang Hung Pham[a, b], Martin Gagnon[c], Jérôme Antoni[b], Antoine Tahan[a], Christine Monette[d]

[a] École de technologie supérieure (ÉTS), H3C 1K3, Montreal, QC, Canada
[b] University of Lyon, INSA Lyon, Laboratoire Vibration Acoustique, F69621, Villeurbanne, France
[c] Institut de recherche d'Hydro-Québec (IREQ), J3X1S1 Varennes, QC, Canada
[d] Andritz Hydro Canada Inc, H9R 1B9, Point-Claire, QC, Canada

Contact : quang-hung.pham.1@ens.etsmtl.ca or quang-hung.pham@insa-lyon.fr

Abstract

The measurement of stress/strain on blade plays an essential role in the fatigue assessment of the hydroelectric turbine runner. However, a typical measurement campaign does not cover all the possible operating conditions due to the field measurement requirements and limitations, which leads to fatigue evaluation missing for unmeasured conditions. In this paper, kriging interpolation method is used to estimate the missing fatigue information based on the available measured operating conditions of the turbine. The rainflow counting matrix, which contains the fatigue cycles of strain signal, is considered as the input of the interpolation process. For validation, the fatigue cycles are randomly generated, using bivariate Gaussian distributions, from the interpolated matrix for comparison with the experimental values under similar operating conditions. The developed approach will help plan experimental campaign and might contribute to decreasing the measurement requirements for runner fatigue assessment.

Keywords: Hydroelectric turbine; Kriging interpolation; Runner fatigue assessment; Rainflow counting

Nomenclature

B	Bin value of ARM histogram [probability]
f	From value of a strain cycle [µstrain]
t	To value of a strain cycle [µstrain]
o	Operating condition [%OV]
p	Bin position ($p(f,v)$)
n_o	Number of experimental operating conditions
ϑ_i	Set of bin position p_i and its neighbours
λ_{kl}	Regression weight
σ_e^2	Error variance
γ	Semivariogram value
$\hat{\gamma}$	Experimental Semivariogram
h	Histogram Space Increment
u	Operating Conditions Increment
$v(h,u)$	Set of paired points
$N(h,u)$	Cardinal of $v(h,u)$
$L(.)$	Lagrange function
μ	Lagrange multiplier
$\gamma_{Smetric}$	Sum-metric semivariogram model
γ_{joint}	Joint semivariogram

ARM	Asymmetric Rainflow Matrix
BEP	Best Efficiency Point
BGD	Bivariate Gaussian Distribution
CFD	Computational Fluid Dynamic
DC	Decreasing Cycle
DPL	Deep Part-Load
ES	Experimental Semivariogram
FEA	Finite Element Analysis
FPC	Four-Points Counting
HCF	High Cycle Fatigue
IC	Increasing Cycle
MAE	Mean Absolute Error
RMSE	Root Mean Square Error
SNL	Speed No-Load
STK	Spatio-Temporal Kriging
%OV	Guide Vane Opening Level
κ	Anisotropy correction
γ_o	Semivariogram model for variable o
γ_p	Semivariogram model for variable p

1. Introduction

Fatigue is one of the damage mechanisms occurring during the operation of a hydroelectric turbine. Today, runner blades are experiencing increasing dynamic strains due to larger operating range of turbines caused by electrical network usage changes [1]. These changes mean that the turbine must

operate under conditions that deviate significantly from the Best Efficiency Point (BEP), which leads to a higher risk of fatigue crack. Monette et al. (2016) highlighted the reduced fatigue life of turbine runner and the high repair costs generated by this enlarged operating range [1]. A general overview of conditions and dynamic phenomena that significantly influence runner fatigue is presented by Liu et al. (2016), Seidel et al. (2014) and Gagnon et al. (2014) [2-4]. Steady state operating conditions containing a high stochastic component such as Speed No-Load (SNL) or Deep Part-Load (DPL) or Part load containing vortex rope phenomenon, and transient conditions such as turbine start-up can have major impact on runner fatigue assessment if not properly accounted for.

Fatigue is assessed based on several factors (runner material, stress level, initial crack), and requires a representative strain/stress history. Many approaches are available for improving runner fatigue life estimation. To limit fatigue failure, Gagnon et al. (2013) proposed a runner reliability model using the High Cycle Fatigue (HCF) onset as the limit [5]. Fatigue damage is linked to the propagation of cracks on the runner, and thus, an investigation of the metallurgical or mechanical behaviour of the material is also needed [6-9]. However, fatigue assessment cannot be carried out if the dynamic load information is missing. Computational Fluid Dynamic (CFD) combined with Finite Element Analysis (FEA) can be used to estimate the static and dynamic behaviour of the structure under such as SNL or DPL [10-12]. Nevertheless, numerical prediction is still challenging when turbulence models are not able to properly describe the behaviour of the turbine [13]. Moreover, the validation of numerical simulation depends on the availability of the experimental information. However, to recover this missing experimental information, other approaches, such as the interpolation and extrapolation of experimental data, can be used [14-16]. The use of indirect method can also help minimize the measurement requirement, Diagne et al. (2016) utilised the ARMAX (Autoregressive Moving Average with eXogenous input) model to predict the runner dynamic stress using shaft torsion information, which is more readily available [17]. For a detailed review of the fatigue life estimation methodologies used for Francis turbines, please refer to Presas et al. (2019) [13]. Our state-of-art summary shows that in situ field strains/stress during or after commissioning provide important and essential information for the study of the hydroelectric turbine runner fatigue.

Finding a solution that can provide missing experimental information and improve knowledge on the dynamic behaviour remains a challenge. Obtaining experimental strains over all the possible states of the hydroelectric turbine operation would be overly costly and time-consuming; hence, experimental measurements are usually limited to a limited set of operating conditions, which leads to difficulties during runner fatigue assessment. The goal of this paper is to propose a methodology to minimize the requirements for experimental strain measurements. There are three difficulties associated with the measurement of strain for fatigue evaluation:

- Limited number of measured locations on runner blades
- Limited measurement length
- Limited number of measured operating conditions

The first was studied by Salah where the kriging method was used for the interpolation between different locations of the runner blade [14]. For the second, several approaches can be used for temporal extrapolation to obtain long-term fatigue assessments. Poirier et al. (2016) [15] extrapolated information on the cyclostationary decompositions of the short-term records of strain signals to evaluate runner fatigue cycles over a longer period of usage. Other researchers extrapolated the rainflow matrices directly over longer periods [19-22]. However, such strain interpolation between blade locations or a temporal extrapolation can be performed if and only if an estimate of the signal is available (generally in the form of measurements) at a given turbine operating condition. Therefore, the lack of measurements over the complete operating range should be studied as shown in *Figure* 1.

In a previous work the authors developed an interpolation process for a subcomponent of the strain signal between different turbine operating conditions [16]. Only the periodic component of the signal was interpolated while the complete strain signal was overlooked as it is more complex and contains other hidden structures. The direct interpolation of complete strain signal (measurement form) is a complicated problem because of these hidden structures. However, in cases where only fatigue information is needed for further evaluation, the strain signal could be transformed into a cycle counting form (level crossing, peak counting, rainflow matrices, etc.) to simplify the interpolation. Among cycle counting methods, the rainflow algorithm is commonly used for fatigue assessment of

hydroelectric turbines [1, 10-11, 15-16]. Therefore, our goal is to interpolate the rainflow counting matrices (instead of the signal itself), which contain information on the fatigue cycles, over the complete range of operating conditions. Notice that there are two important variables that define the operating conditions of turbine: opening vane level and head level. However, in this study, the aim is to focus on the differences of stress level between different opening vane levels for the same head (the data in the case study also comes from the measurements strain at relatively constant head). The head level might be used in the future research if observed data become available for multiple head levels.

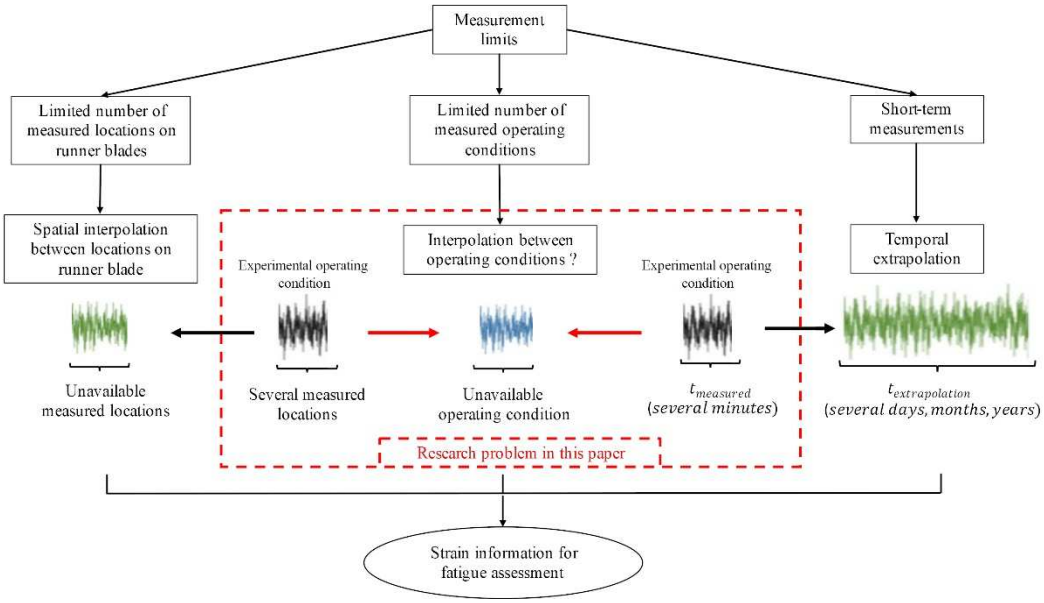

Figure 1. Measurement limits and interpolation/extrapolation solutions for the fatigue assessment of hydroelectric turbine runner

The kriging method was chosen for this study to interpolate rainflow counting matrices (histogram form), Then, the fatigue cycle reconstruction was generated via stochastic simulations using bivariate Gaussian distributions. This reconstruction step helps recover the long-term information of fatigue, more cycles are generated, more fatigue information is evaluated. The obtained results were compared with the experimental fatigue cycles to evaluate the correctness of the proposed interpolation methodology. In addition, the signal was reconstructed from the simulated cycles by using the inverse method proposed in [19-20] to compare with the measured signal.

The paper is organized as follows: First, the methodology is presented with detailed explanations of the principal methods (rainflow-counting, kriging interpolation, reconstruction simulation). Then, a hydroelectric turbine runner case study is presented followed by interpolation results and a discussion.

2. Proposed Methodology

2.1 Asymmetric Rainflow Counting Matrices

The rainflow algorithm allows the analysis of signal amplitudes (or range) by assigning extreme (max, min) values of closed loading cycles. To evaluate fatigue, only the range/amplitude information of each cycle is often needed. In this study, the strain signal is transformed into an Asymmetric Rainflow Matrix (ARM), which separates the cycles into two types: increasing and decreasing cycles (or standing and hanging cycles in some references) [24]. These two types of cycles are defined based on the order of occurrence of maximum and minimum values in the signal. To construct the ARM, a rainflow-counting procedure called the Four-Point Counting (FPC) algorithm is used [25]. Considering four consecutive points (three consecutive cycles) in the loading signal, if the cycle range created by the second and the third points is smaller than the range of the two other points, this cycle is reduced and is added to the ARM. An ARM is constructed by two variables: from value (noted as *f*) corresponding to the amplitude of the first point of the cycle (the first point of the cycle arrives on the axis of time) and to value (noted as *t*) corresponding to the amplitude of the final point of the cycle (*Figure 2*). In our study, the created ARM is represented under histogram density form where each bin contains the number of cycles or the probability of occurrence of cycles. The ARM is a

composition of max-min cycles (above the matrix diagonal) and min-max cycles (below the matrix diagonal). Furthermore, the choice of the asymmetric rainflow matrix allows a distinction to be made between increasing and decreasing cycles during the signal reconstruction. To properly apply the FPC, the turning points, which represent the peak and the valley of the signal, are extracted before the ARM is constructed. This extraction deletes variations that are neither peaks nor valleys (these small variations in the rainflow approach are considered to have minor impact on the fatigue assessment).

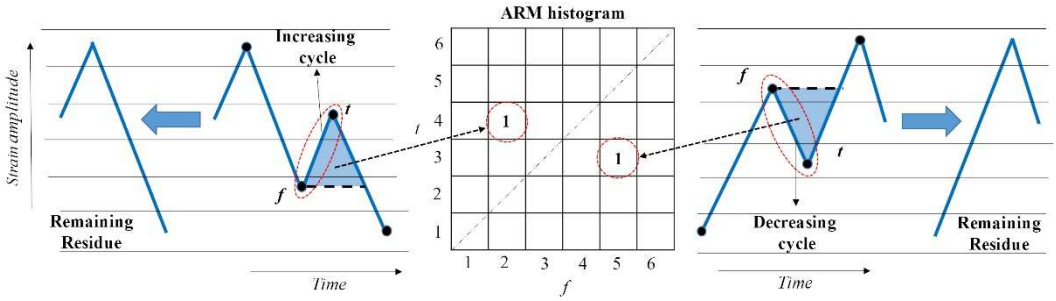

Figure 2. Four Point Counting algorithm applied for strain signal.

2.2 *Kriging Interpolation Method*

Before presenting the interpolation method, the context must be clarified. The interpolation input is a set of ARM histograms, which are spread across the different turbine operating conditions. The histogram bins are fixed for all the histograms. The goal is to estimate new ARM histograms at any given operating conditions (see *Figure 3).*

The relation between the bins of each ARM matrix is an important bit of information that cannot be ignored in the interpolation phase. Hence, the kriging interpolation method is a suitable method to preserve the spatial covariance within the ARM histogram. However, there is also a covariance to preserve between each operating condition. Thus, a multivariate kriging method, inspired by Spatio-Temporal Kriging (STK), where the temporal and spatial coordinates are treated separately, is applied, and developed for this study. Readers can consult the general definition of the kriging principle in [27-30].

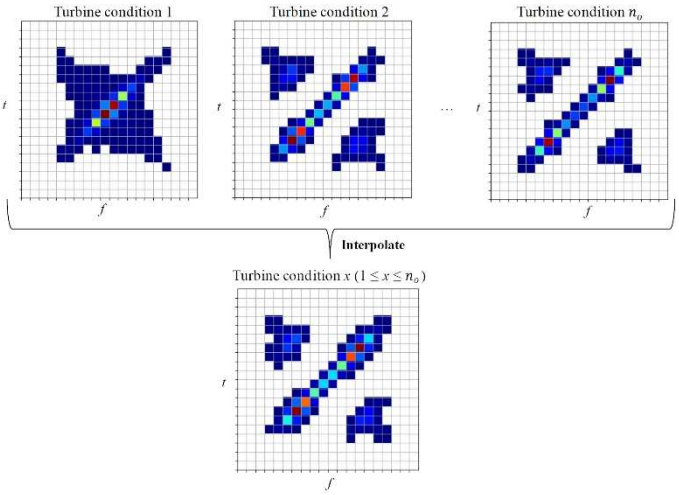

Figure 3. Interpolation objective: new ARM histogram (at a given turbine operating condition) is interpolated from all experimental ARM histograms

In our case, the position of bins in the ARM histogram and the operating condition are considered as coordinates. The estimator used in this study can be written as:

$$B^*(p_i, o_x) = \sum_{k \in \vartheta_i} \sum_{l=1}^{n_o} \lambda_{kl}(p_i, o_x) B(p_k, o_l) \quad (1)$$

where p_i is a given bin position in the ARM histogram (p depends on a 'from value' f_i and a 'to value' t_i : $p_i(f_i, t_i)$, o_x is a given operating condition of the turbine, $B^*(p_i, o_x)$ is the interpolated

value of bin p_i at the condition o_x, $B(p_k, o_l)$ is the known bin value at location (p_k, o_l), $\lambda_{kl}(p_i, o_x)$ is the regression weight to optimize during the interpolation process (details below), n_o is the number of experimental turbine conditions, ϑ_i is a set of neighbourhood positions of p_i (including p_i) . It must be noted that the spatial covariance map is obtained from the whole histograms of all the experimental turbine conditions, while Eq. 1 searches for the input in the neighbourhood ϑ_i of the target bin. This reduces the calculation time and avoids the interpolation smoothing effect.

Kriging allows the unbiased estimation of values at given locations by determining the weights λ_{kl} which minimize the error variance $\sigma_e^2(p_i, o_x)$ between the real value B and the interpolated value B^* at the same location, $\sigma_e^2(p_i, o_x) = Var\big(B(p_i, o_x) - B^*(p_i, o_x)\big)$. The condition for non-bias relating to the regression weights is $\sum_{k\in\vartheta_i}\sum_{l=1}^{n_o}\lambda_{kl}(p_i, o_x) = 1$; it ensures a constant local mean value in every location. Therefore, to impose this non bias constraint, the minimization system is updated by adding a Lagrange parameter μ:

$$L(\lambda_{kl}, \mu) = \underbrace{Var\big(B(p_i, o_x) - B^*(p_i, o_x)\big)}_{\sigma_e^2(p_i, o_x)} + 2\mu\left(\sum_{k\in\vartheta_i}\sum_{l=1}^{n_o}\lambda_{kl}(p_i, o_x) - 1\right) \tag{2}$$

where $L(\lambda_i, \mu)$ is the Lagrange function. Making use of Eq.1, the minimization of Eq.2 leads to the system that allows to obtain the λ_{kl} and μ:

$$\begin{cases} \sum_{k\in\vartheta_i}\sum_{l=1}^{n_o}\lambda_{kl}(p_i, o_x)\,\gamma(h_{\|p_k - p_j\|}, u_{|o_l - o_m|}) - \mu = \gamma\left(h_{\|p_i - p_j\|}, u_{|o_x - o_m|}\right),\ j \in \vartheta_i,\ m = 1, \dots, n_o \\ \sum_{k\in\vartheta_i}\sum_{l=1}^{n_o}\lambda_{kl}(p_i, o_x) = 1 \end{cases} \tag{3}$$

where

$$\gamma\big(h_{\|p_a - p_c\|}, u_{|o_b - o_d|}\big) = 0.5 \times Var[B(p_a, o_b) - B(p_c, o_d)] \tag{4}$$

is the semivariogram, which depends on the increments h and u, p_a and p_c are two positions of the bin in the histogram, o_b and o_d are two turbine operating conditions such that: $h = \|p_a - p_c\|$ and $u = |o_b - o_d|$. Based on Eq. 4, the semivariogram is defined as the half variance between two values separated by the increments h and u. This semivariogram can be considered as a simpler representative of the covariance map that does not require information on the mean value of B (that is often unknown in practice [29]). To obtain the semivariogram at any possible increment (h, u), some numerical models can be used to fit to the semivariogram using analysis estimations (e.g., Least Squares method) [27][30]. However, to choose the best numerical model, one needs to create a semivariogram from the experimental data. In practice, the quantity of data is not enough to provide values exactly separated by $h = \|p_a - p_c\|$ and $u = |o_b - o_d|$, as in Eq. 4. Consequently, to create the Experimental Semivariogram (ES), Eq. 5 is used. This equation allows an estimation of the semivariogram value associated with a set of (h, u) values, where h and u are midpoints of imposed spatial increment intervals:

$$\hat{\gamma}(h, u) = \frac{1}{2N(h, u)}\sum_{(a,b,c,d)\in\upsilon(h,u)}[B(p_a, o_b) - B(p_c, o_d)]^2 \tag{5}$$

where $\hat{\gamma}(h, u)$ is the experimental semivariogram, $\upsilon(h, u)$ is a set of paired points separated such that $\|p_a - p_c\| \in [h - dh, h + dh]$ and $|o_b - o_d| \in [u - du, u + du]$ with dh > 0, du > 0, $N(h, u)$ is cardinal of $\upsilon(h, u)$. The next step is to fit the ES with a numerical model that will make a continuity throughout the increments for the semivariogram. Classes of semivariogram models are presented in [29-30]. For example, the sum-metric model (*Figure 4)*, which turns out as one of the best fitting models in our study, is expressed as:

$$\gamma_{Smetric}(h, u) = \gamma_p(h) + \gamma_o(u) + \gamma_{joint}\big(\sqrt{h^2 + (\kappa.u)^2}\big) \tag{6}$$

where $\gamma_p(h)$ is the univariate semivariogram model for the variable p, $\gamma_o(u)$ is the univariate semivariogram for the variable o, and $\gamma_{joint}\big(\sqrt{h^2 + (\kappa.u)^2}\big)$ is a metric joint variogram model including an anisotropy correction κ [30]. Many basic analytical models exist for the univariate semivariograms such as spherical model, the exponential model, the Gaussian model, power model,

etc. [14][27]. The schema in *Figure* 5 summarizes the kriging interpolation approach used in our case study.

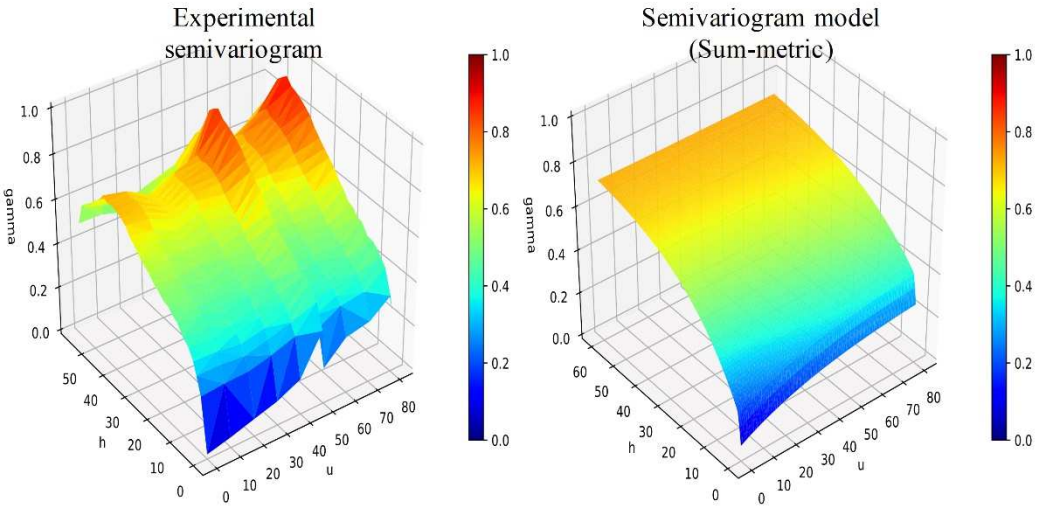

Figure 4. Experimental semivariogram and example of semivariogram model (Sum-metric). Semivariogram values in this figure are normalized.

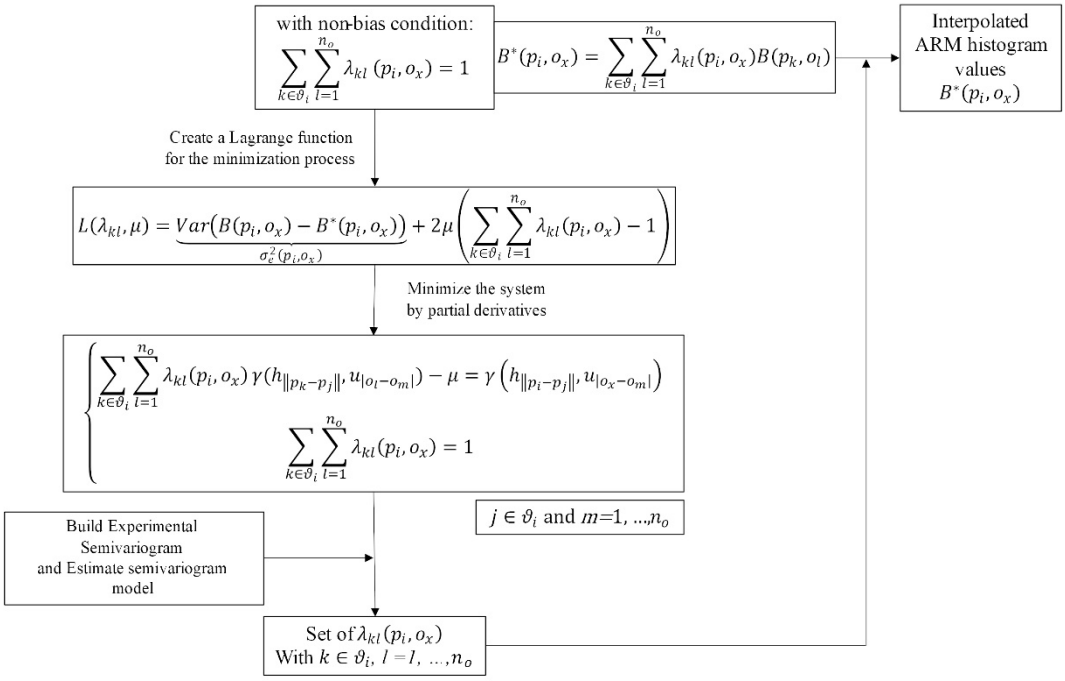

Figure 5. Schema of the Kriging process in this paper applied for the studied variables

2.3 Simulation Reconstruction

To generate strain cycles from an interpolated ARM histogram, it must be converted to a continuous distribution. A smoothing process for the interpolated histogram is proposed by considering that the cycles inside each bin follow a Bivariate Gaussian Distribution (BGD). The BGD mean corresponds to the coordinates of the center point of the bin and the proposed covariance matrix is $\sigma^2\mathbf{I}_2$, where $\sigma = \frac{0.5\times bin\ diagonal}{variability\ parameter}$ and $\mathbf{I}_2$ is the identity matrix. The variability parameter in the denominator is a coefficient proposed to ensure that the simulated cycle distribution does not create too much variability outside its bin. A variability test is proposed to select this variability parameter. In this study, since the interpolation input comes from the experimental strains measured by gauges, we impose the strain gauge uncertainty as a limited level of variability, which limits the variability of

generated point outside each bin. For example, if the relative error of the strain gauge is ±y%, the imposed limited level for the variability will be y%. It must be noted that the experimental uncertainties are not the focused problem of this study. The test of variability is then launched for several variability parameters. For each ARM, Monte Carlo simulation is generated from the bivariate normal distribution with the mean [0,0] and the covariance $\sigma^2\mathbf{I}_2$. If the percentage of the sample values outside the bin dimension is approximately equals to the limited level y% (*Figure* 6), this variability parameter is chosen for the ARM histogram smoothing process. The reader can also optimize the variability parameter by using or adding other uncertainty types (e.g., error of kriging interpolation) if needed for other study. In addition, other approaches, such as the Kernel Density Estimation (KDE), can also be useful for smoothing the histogram [19-20]. Finally, the cycles are randomly generated from the set of BGDs by respecting the probability of occurrence of cycles in each bin (the sum of all the probability values in the histogram is equal to 1).This generation process allows an observation of a set of simulations, which is useful for the industry when evaluating the fatigue. The risk of fatigue will be predicted with a set of possibilities instead of a unique prediction.

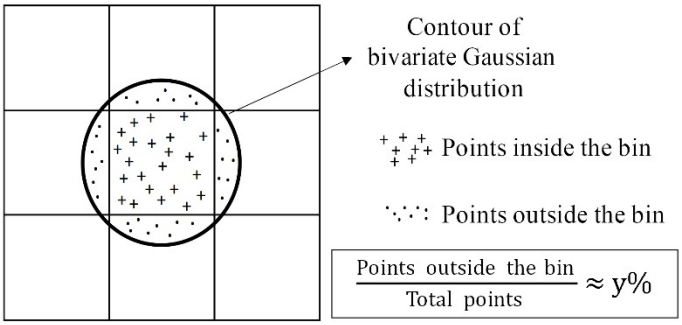

Figure 6. Percentage of the sample values outside the bin dimension is approximately equal to y%

In addition, an inverse method is used to reconstruct the strain signal from the simulated samples [19-20]. The signal reconstruction consists of two steps: First, the largest cycles (the furthest points from the ARM diagonal), either a Decreasing Cycle (DC) or an Increasing Cycle (IC), are used to create an initial reconstructed signal (also called the *remaining residue* in *Figure 2*). Second, all the other cycles are randomly inserted into the remaining residue descending order (from the furthest to the closet point from the diagonal) by respecting the rule proposed by Socie et al. [19-20]. The smaller IC is added to the position of the larger DC (peak and valley values of the smaller cycle fall within the range of the larger cycle) and vice versa. Each cycle added to the remaining residue is removed in the ARM until there are no cycles left. It is not expected that the reconstructed signal will be similar to the experimental one because only the rainflow information is considered for the interpolation; nevertheless, the signal should represent a time history that generates equivalent fatigue damage. The flowchart in *Figure 7* illustrates the interpolation scheme used in this study.

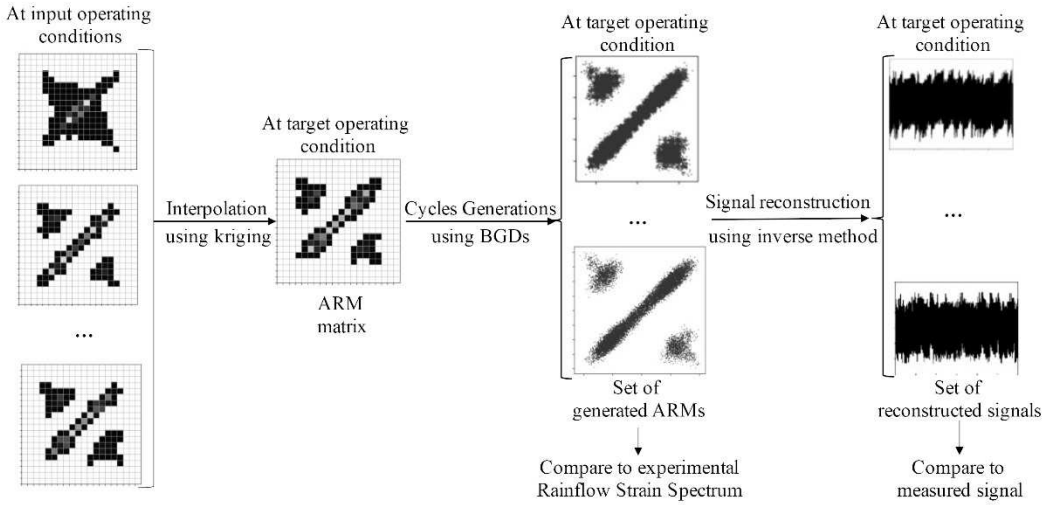

Figure 7. Flowchart displays the interpolation scheme

3. Case Study

The data used in this case study were obtained from experimental measurements conducted using strain gauges, which were installed on the runner blade of a Francis hydroelectric turbine of a power plant in Quebec (Canada). The measured locations on the blade are close to critical locations where the highest stress levels are found. For the purpose of this paper, the experimental uncertainties (ambiance error, human error, error of installation, etc.) are ignored. The interpolation is performed between different

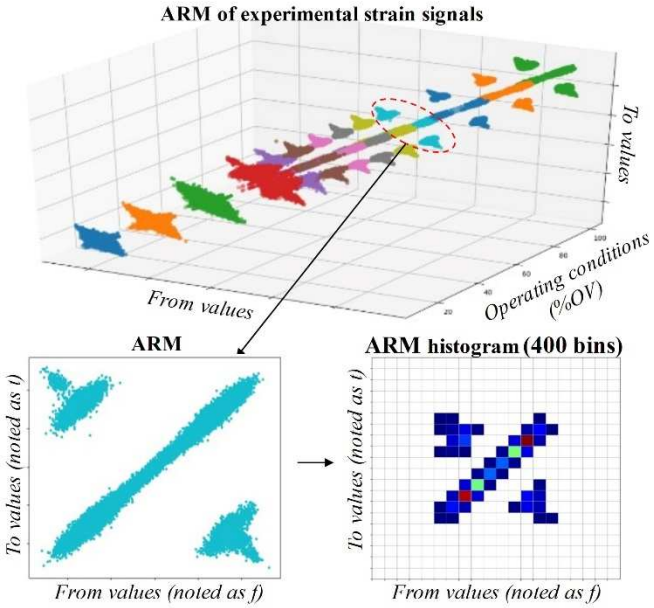

Figure 8. ARMs over different operating conditions for this case study and example of ARM histogram (the white bin corresponds to the null value)

steady-operating conditions of the turbine. Transient operating conditions, such as start-ups or stops, are not considered in this research because their specific dynamic behaviours do not correlate with steady-operating conditions. A steady-operating condition is approximately defined as a regime of the turbine under which the guide vane opening, power and turbine head can be considered as quasi constant. For the interpolation, steady states are separated by different opening levels of the turbine guide vane (noted as %OV) (*Figure 8*). The guide vanes control the flow rate into the runner.

Due to the high quantity of cycles in each strain signal, the ARMs are presented under the histogram density form with a prior fixed bin number where each bin contains the probability of occurrence of cycles (*Figure 8*). The choice of input/output bin number is an important parameter. A higher number of bins significantly increases the calculation time, while a smaller one leads to

imprecise results because of the large interval of values covered by each bin.

Fitting a model to the experimental semivariogram is an important step of the interpolation process. We highly recommend using the cross-validation technique for this step [29]. This technique removes some point values in the input set and then predicts these values from the remaining points using fitted semivariogram models. This procedure is repeated several times for each semivariogram model to observe the interpolation performance of this model. Moreover, other error estimations such as Root Mean Square Error (RMSE) or Mean Absolute Error (MAE) are additionally used to obtain the best semivariogram model. In our case study, based on a good cross-validation performance (*Figure 9*) and on the small error estimation values (see MAE and RMSE in *Table 1*), the chosen semivariogram model was sum-metric model (see Eq. 6 and *Table 1*). For each univariate model, $\gamma_p(h)$ was modeled by sum of an exponential model and a Gaussian model, $\gamma_o(u)$ and $\gamma_{joint}\left(\sqrt{h^2+(\kappa.u)^2}\right)$ was respectively modeled by a Gaussian and an exponential model (*Table 1*).

$$\begin{cases} \gamma_{exponential}(h) = (Sill - nu).\left(1 - e^{-\frac{3.h}{range}}\right) + nu \\ \gamma_{Gaussian}(u) = (Sill - nu).\left(1 - e^{-\frac{(3.u)^2}{range^2}}\right) + nu \end{cases} \quad (7)$$

where $Sill$ corresponds to the average variance where the experimental semivariogram stabilizes, *range* presents the distance from which no more correlations exist between the data, and nu is a small value added to the sill parameter to represent a very short-range variability in the dataset (Nugget effect) [14][27].

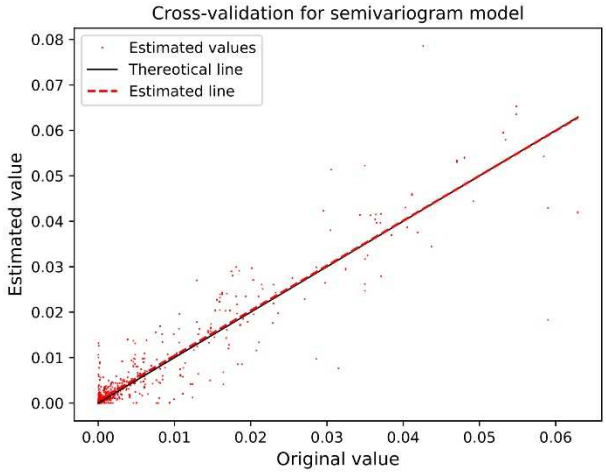

Figure 9. Cross validation performance of sum-metric model (its parameters are presented in Table 1)

The neighbourhood set ϑ_i (Eq. 1) is chosen using the cross-validation technique. Several sets with different numbers of neighbourhood positions are tested and the optimized set is chosen based on the smallest RMSE and based on the similarity between theoretical and estimated line (see APPENDIX). Notice that the set of neighbourhoods is applied only for the histogram position "*p*", but not for operating conditions "*o*". Thus, the points in a neighbourhood set correspond to the closest points from the target points in ARMs. In this case study, the set of 9 nearest positions is chosen for the neighbourhood set ϑ_i in Eq. 1 (see APPENDIX).

Table 1 shows the optimized parameters used for this case study. To verify the quality of the interpolated result, a validation is made using known experimental operating conditions (not included in the set of interpolation inputs).

Parameters	Semivariogram model parameters (fitted to normalized ES- see *Figure 4*)					
Input/Output histogram bins number:	Optimized sum-metric model (RMSE = 0.0993, MAE= 0.0747) Eq. 6: $\gamma_{Smetric}(h,u) = \gamma_p(h) + \gamma_o(u) + \gamma_{joint}\left(\sqrt{h^2+(\kappa.u)^2}\right)$					
		Model type	*Sill*	nu	*range*	κ

40 × 40 bins Input operating conditions (%OV): 11, 20, 40, 50, 60, 70, 90, 100 Variability para. ≈ 3.87 Number of points in neighbourhood set: 9	$\gamma_p(h)$	Gaussian	0.116	3e-08	2.011	0.296
		Exponential	0.376	0.009	70.025	
	$\gamma_o(u)$	Gaussian	0.040	0.042	30.007	
	$\gamma_{joint}\left(\sqrt{h^2 + (\kappa.u)^2}\right)$	Exponential	0.230	7e-08	60.057	

Table 1. Parameters of the proposed interpolation process adapted for the case study dataset

4. Results and Discussions

The interpolated results (corresponding to each step illustrated in *Figure 7*) and their comparison with experimental ones at 55% OV are presented in the *Figures 10-12*. All the results are normalized to respect the confidential information.

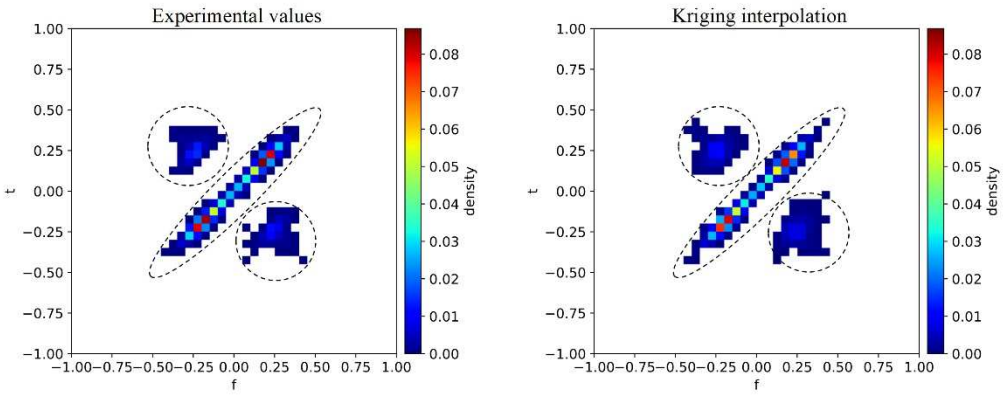

Figure 10. Comparison between experimental and Interpolated ARM histogram at 55% OV

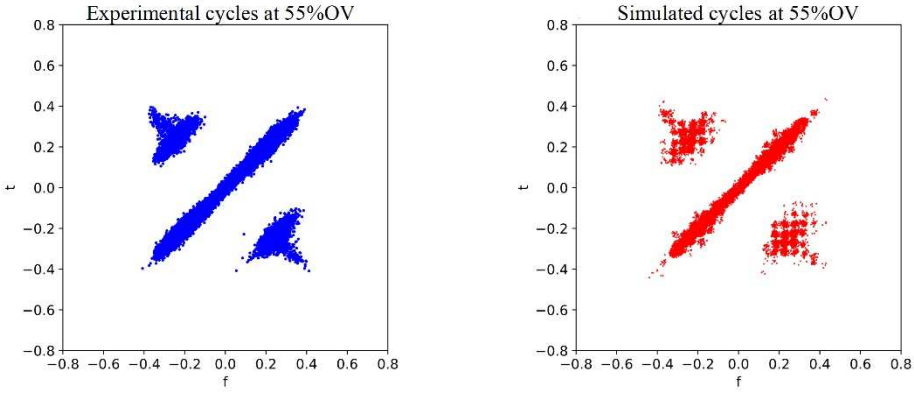

Figure 11. Experimental and generated cycles (one simulation) at 55 %OV

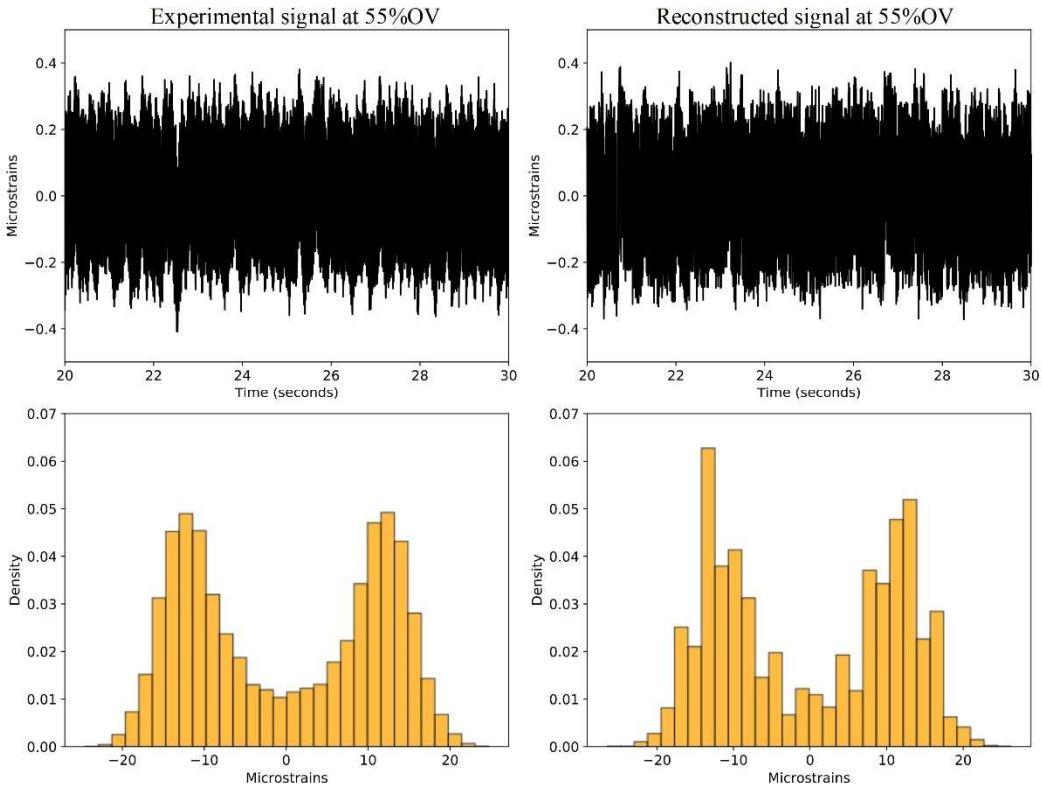

Figure 12. Comparison between experimental signal and one reconstructed signal at 55 %OV. Above: 10 seconds of signals. Below: Histogram of whole signal

The interpolated ARM shows the same number of distribution modes (dashed line in *Figure 10*) as in the experimental ones; this means that this interpolation did not generate large overestimation in positions the null bins. Nonetheless, some differences are observed at the frontier positions of each mode in the interpolation result (*Figure 10, 11*). Graphically, the reconstructed signal (*Figure 12*) is not similar to the experimental one like we have foreseen, however its amplitudes have the same level as the experimental one. To verify the quality of interpolation process, we have compared the rainflow strain spectrums (strain range as a function of cumulative number of fatigue cycles) between 500 simulations (sampled from the set of BGDs) and the experimental values at some operating conditions (*Figure 13*).

For fatigue assessment, the expected goal in this study is to capture the amplitude/range level of fatigue cycle (especially high range cycles which cause more damage). At 55 %OV and 65 %OV, the experimental rainflow (the blue line in *Figure 13*) is mostly within of the set of simulations while there seems to be some overestimations at the high ranges at 80 %OV. This difference might be explained by that there are more operating conditions close to the 55 %OV, 65 %OV in the interpolation input set (see *Table 1)*.

An unusual variability is observed at 30 %OV. The interpolation result depends on the nature of known data. The more complicated the combination of phenomena hidden in the signal, the less confident we might be in the interpolation result. Therefore, at some partial load conditions of turbine, this unusual variability of the interpolated result occurs when an operating condition with a complicated dynamic behavior is presented next to the interpolation target condition. Some of those conditions contain specific fluctuation coming from the vortex in the draft tube [3], which appears and disappears over limited set of measured operating conditions rendering the interpolation difficult. This problem provides new challenge for further research, in which we would like to recover such fluctuation information.

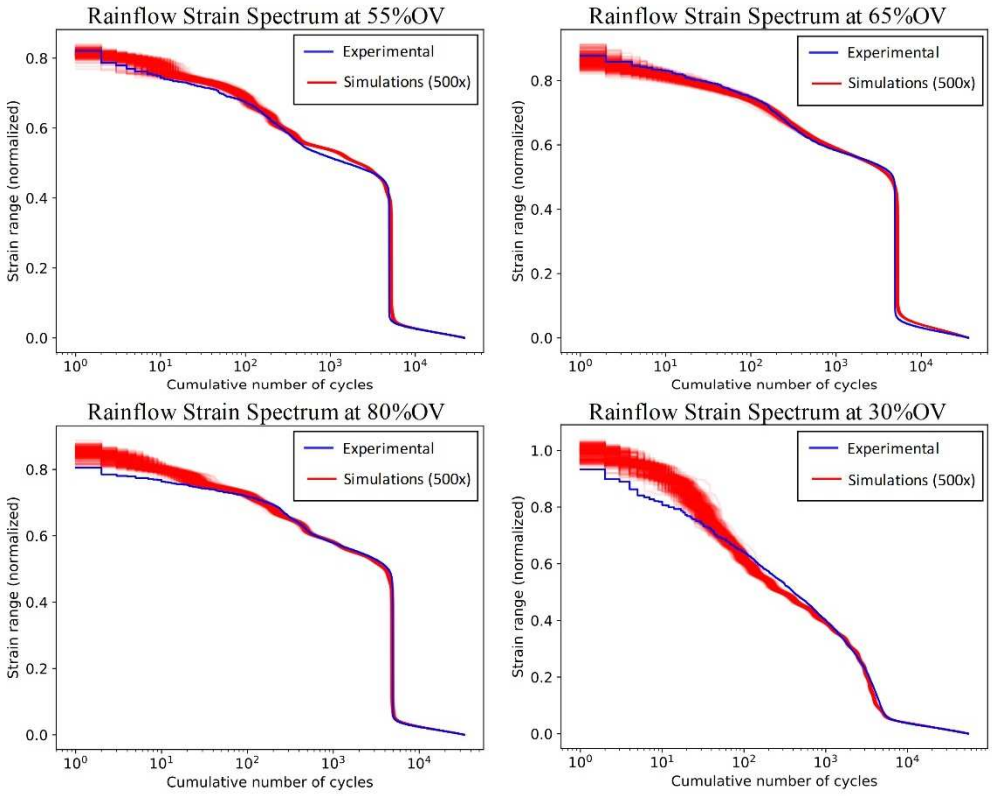

Figure 13. Rainflow strain spectrum between experimental values and simulations

For the runner maintenance strategy, even if the reconstructed signal is not similar to the experimental one (*Figure 12*), the interpolated strain ranges might be more representative of data variability and uncertainty than reusing experimental measurements from nearby operating conditions. Also, the proposed interpolation can be a solution to reduce the measurement requirements for runner fatigue assessment.

5. Conclusions

In this article, an interpolation process using kriging has been presented to estimate the strain range at any steady state operating condition based on rainflow cycle counting for hydroelectric turbine runner fatigue assessment. A set of bivariate Gaussian distributions were used to smooth the histogram, allowing quicker simulations of the loading cycles. It must be noted that the proposed interpolation process is sensitive to the parameters used (i.e., the semivariogram model, etc.), using the error optimizing methods (such as cross-validation, Mean Absolute Error, etc.) are therefore highly recommended. The results of the case study show that even when the reconstructed signal is not similar to the experimental one, our proposed interpolation might be useful to estimate the dynamic strain level using only the load cycles information of strain signal.

The advantage of the proposed method is that it creates a stochastic process accounting for uncertainty hence contributing to fatigue risk assessment by generating loading cycles representative of observed behaviours. Moreover, it can help to optimize the requirements for experimental measurements.

In the result of this case study, the complicated phenomena hidden in strain signal caused the unusual variability at some partial load conditions. For further research, preserving other information of strain signal (not only the strain range information) during the interpolation phase will be interested to improve the quality of missing data recovery at unmeasured operating conditions.

Acknowledgments

The author would like to thank the Hydro-Québec Research Institute (IREQ), Andritz Hydro Canada LTD, INSA de Lyon (France), École de Technologie Supérieure de Montréal (Quebec, Canada) and the Mitacs Acceleration program for their support and financial contribution.

About 4410 words (excluding abstract, figure captions and references). Figure 10, 13 must be printed in color

References

[1] Monette, C., Marmont, H., Chamberland-Lauzon, J., Skagerstrand, A., Coutu, A., & Carlevi, J. (2016, November). Cost of enlarged operating zone for an existing Francis runner. In *IOP Conference Series: Earth and Environmental Science* (Vol. 49, No. 7, p. 072018). IOP Publishing.

[2] Liu, X., Luo, Y., & Wang, Z. (2016). A review on fatigue damage mechanism in hydro turbines. *Renewable and Sustainable Energy Reviews*, *54*, 1-14.

[3] Seidel, U., Mende, C., Hübner, B., Weber, W., & Otto, A. (2014). Dynamic loads in Francis runners and their impact on fatigue life. In *IOP conference series: earth and environmental science* (Vol. 22, No. 3, p. 032054). IOP Publishing.

[4] Gagnon, M., Tahan, A., Bocher, P., & Thibault, D. (2014). Influence of load spectrum assumptions on the expected reliability of hydroelectric turbines: A case study. *Structural Safety*, *50*, 1-8.

[5] Gagnon, M., Tahan, A., Bocher, P., & Thibault, D. (2013). A probabilistic model for the onset of High Cycle Fatigue (HCF) crack propagation: Application to hydroelectric turbine runner. *International Journal of Fatigue*, *47*, 300-307.

[6] Trudel, A., & Sabourin, M. (2014). Metallurgical and fatigue assessments of welds in cast welded hydraulic turbine runners. In *IOP Conference Series: Earth and Environmental Science* (Vol. 22, No. 1, p. 012015). IOP Publishing.

[7] Thibault, D., Gagnon, M., & Godin, S. (2014). Bridging the gap between metallurgy and fatigue reliability of hydraulic turbine runners. In *IOP Conference Series: Earth and Environmental Science* (Vol. 22, No. 1, p. 012019). IOP Publishing.

[8] El Haddad, M. H., Topper, T. H., & Smith, K. N. (1979). Prediction of non propagating cracks. *Engineering fracture mechanics*, *11*(3), 573-584.

[9] Kitagawa, H. (1976). Applicability of fracture mechanics to very small cracks or the cracks in the early stage. *Proc. of 2nd ICM, Cleveland, 1976*, 627-631.

[10] Nennemann, B., Morissette, J. F., Chamberland-Lauzon, J., Monette, C., Braun, O., Melot, M., ... & Giroux, A. M. (2014). Challenges in dynamic pressure and stress predictions at no-load operation in hydraulic turbines. In *IOP conference series: earth and environmental science* (Vol. 22, No. 3, p. 032055). IOP Publishing.

[11] Morissette, J. F., Chamberland-Lauzon, J., Nennemann, B., Monette, C., Giroux, A. M., Coutu, A., & Nicolle, J. (2016, November). Stress predictions in a Francis turbine at no-load operating regime. In *IOP Conference Series: Earth and Environmental Science* (Vol. 49, No. 7, p. 072016). IOP Publishing.

[12] Xiao, R., Wang, Z., & Luo, Y. (2008). Dynamic stresses in a Francis turbine runner based on fluid-structure interaction analysis. *Tsinghua Science and Technology*, *13*(5), 587-592.

[13] Presas, A., Luo, Y., Wang, Z., & Guo, B. (2019). Fatigue life estimation of Francis turbines based on experimental strain measurements: Review of the actual data and future trends. *Renewable and Sustainable Energy Reviews*, *102*, 96-110.

[14] Ben Salah, F. (2014). *Modélisation de la propagation des incertitudes des mesures sur l'aube d'une turbine hydraulique par Krigeage et simulations stochastiques* (Master dissertation, École de technologie supérieure, QC, Canada).

[15] Poirier, M., Gagnon, M., Tahan, A., Coutu, A., & Chamberland-lauzon, J. (2017). Extrapolation of dynamic load behaviour on hydroelectric turbine blades with cyclostationary modelling. *Mechanical Systems and Signal Processing*, *82*, 193-205.

[16] Pham, Q. H., Gagnon, M., Antoni, J., Tahan, A. S., & Monette, C. (2019, July). Interpolation of periodic hidden signal measured at steady-operating conditions on hydroelectric turbine runners. In *SURVISHNO conference,* Lyon, France.

[17] Diagne, I., Gagnon, M., & Tahan, A. (2016, November). Modeling the dynamic behavior of turbine runner blades during transients using indirect measurements. In *IOP Conference Series: Earth and Environmental Science* (Vol. 49, No. 7, p. 072014). IOP Publishing.

[18] Arpin-Pont, J., Gagnon, M., Tahan, S. A., Coutu, A., & Thibault, D. (2012). Strain gauge measurement uncertainties on hydraulic turbine runner blade. In *IOP Conference Series: Earth and Environmental Science* (Vol. 15, No. 6, p. 062042). IOP Publishing.

[19] Socie, D. (2001). Modelling expected service usage from short-term loading measurements. *International Journal of Materials and Product Technology*, *16*(4-5), 295-303.

[20] Socie, D. F., & Pompetzki, M. A. (2004). Modeling variability in service loading spectra. *Journal of ASTM International*, *1*(2), 1-12.

[21] Johannesson, P. (2006). Extrapolation of load histories and spectra. *Fatigue & Fracture of Engineering*

Materials & Structures, *29*(3), 209-217.
[22] Johannesson, P., & Thomas, J. J. (2001). Extrapolation of rainflow matrices. *Extremes*, *4*(3), 241-262.
[23] Matsuishi, M., & Endo, T. (1968). Fatigue of metals subjected to varying stress. *Japan Society of Mechanical Engineers, Fukuoka, Japan*, *68*(2), 37-40.
[24] Johannesson, P. (1999). Rainflow analysis of switching Markov loads. *Lund Institute of Technology, Centre for Mathematical Sciences, Mathematical Statistics, Lund Institute of Technology, Sweden*, 1-27.
[25] Dreßler, K., Hack, M., & Krüger, W. (1997). Stochastic reconstruction of loading histories from a rainflow matrix. *ZAMM-Journal of Applied Mathematics and Mechanics/Zeitschrift für Angewandte Mathematik und Mechanik*, *77*(3), 217-226.
[26] Rychlik, I. (1996). Simulation of load sequences from rainflow matrices: Markov method. *International Journal of Fatigue*, *18*(7), 429-438.
[27] Deutsch, C. V., & Journel, A. G. (1992). Geostatistical software library and user's guide. *New York*, *119*, 147.
[28] Goovaerts, P. (1997). *Geostatistics for natural resources evaluation*. Oxford University Press on Demand.
[29] Montero, J. M., Fernández-Avilés, G., & Mateu, J. (2015). *Spatial and spatio-temporal geostatistical modeling and kriging* (Vol. 998). John Wiley & Sons. (page 266 to 273).
[30] Pebesma, E., & Heuvelink, G. (2016). Spatio-temporal interpolation using gstat. *RFID Journal*, *8*(1), 204-218.
[31] Chiles, J. P., & Delfiner, P. (2009). *Geostatistics: modeling spatial uncertainty* (Vol. 497). John Wiley & Sons, (page 49-54).
[32] WAFO Group. (2017). WAFO–a Matlab toolbox for analysis of random waves and loads, tutorial for WAFO version 2017. *Mathematical Statistics, Lund University*.
[33] Sherman, M. (2011). *Spatial statistics and spatio-temporal data: covariance functions and directional properties*. John Wiley & Sons.
[34] Duda, R. O., Hart, P. E., & Stork, D. G. (2001). Pattern classification 2nd ed. *John Willey & Sons Inc*.

Appendix: The cross-validation performances for several neighbourhood sets

The cross-validation technique was performed for several neighbourhood sets (with the same semivariogram model). The optimized neighbourhood set for the interpolation is chosen based on the smallest RSME and based on the similarity between theoretical (black) and estimated line (red) in the cross-validation. In observing *Figure 14*, if one chooses a small set (the case of 5 points) or a big set (the cases of 35 or 49 points), the variation and the RMSE values are larger. In this case study, the set of 9 neighbourhood points is chosen (row 1 and column 2 in *Figure 14*).

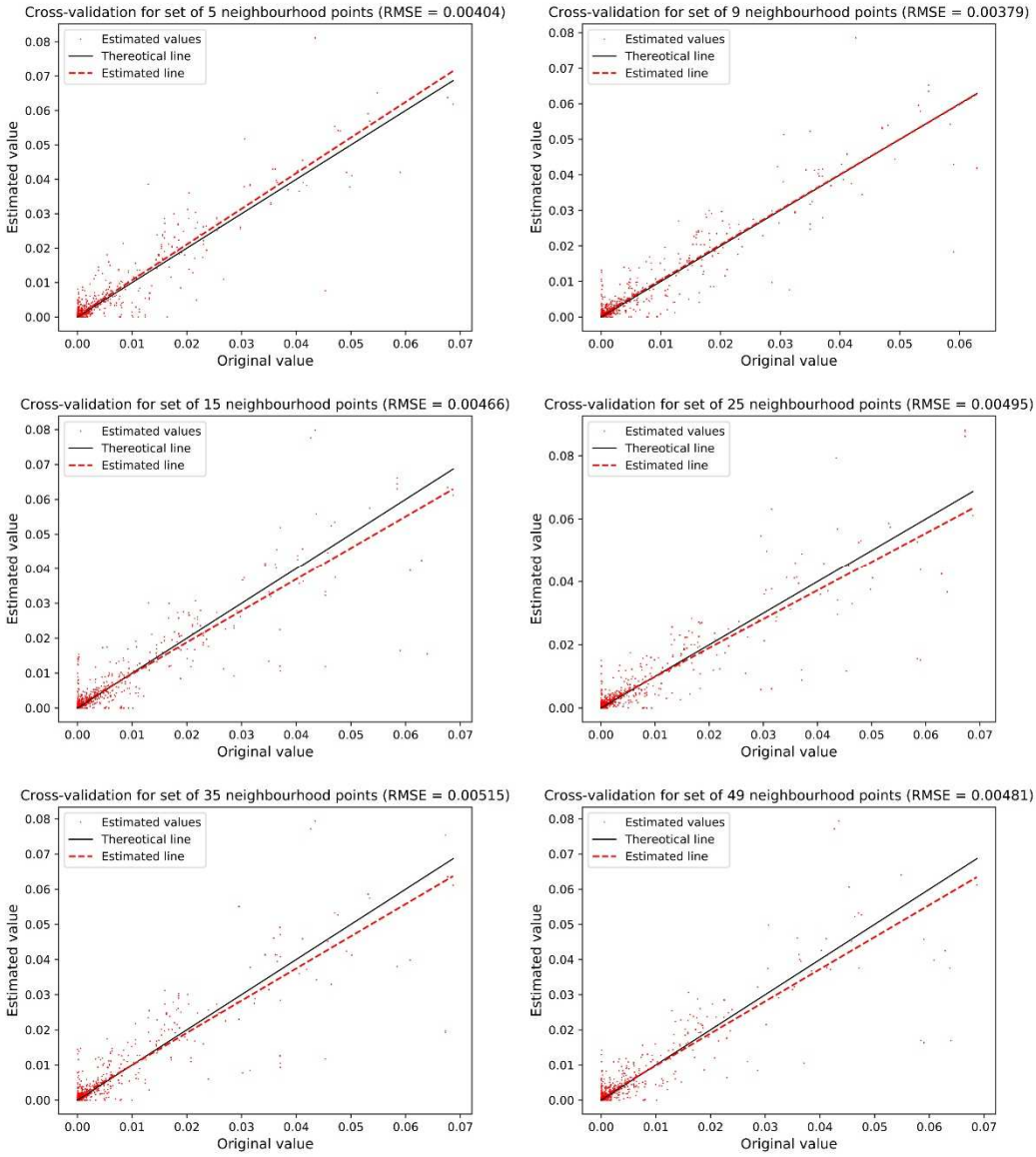

Figure 14. Cross-validation performances for several neighbourhood sets

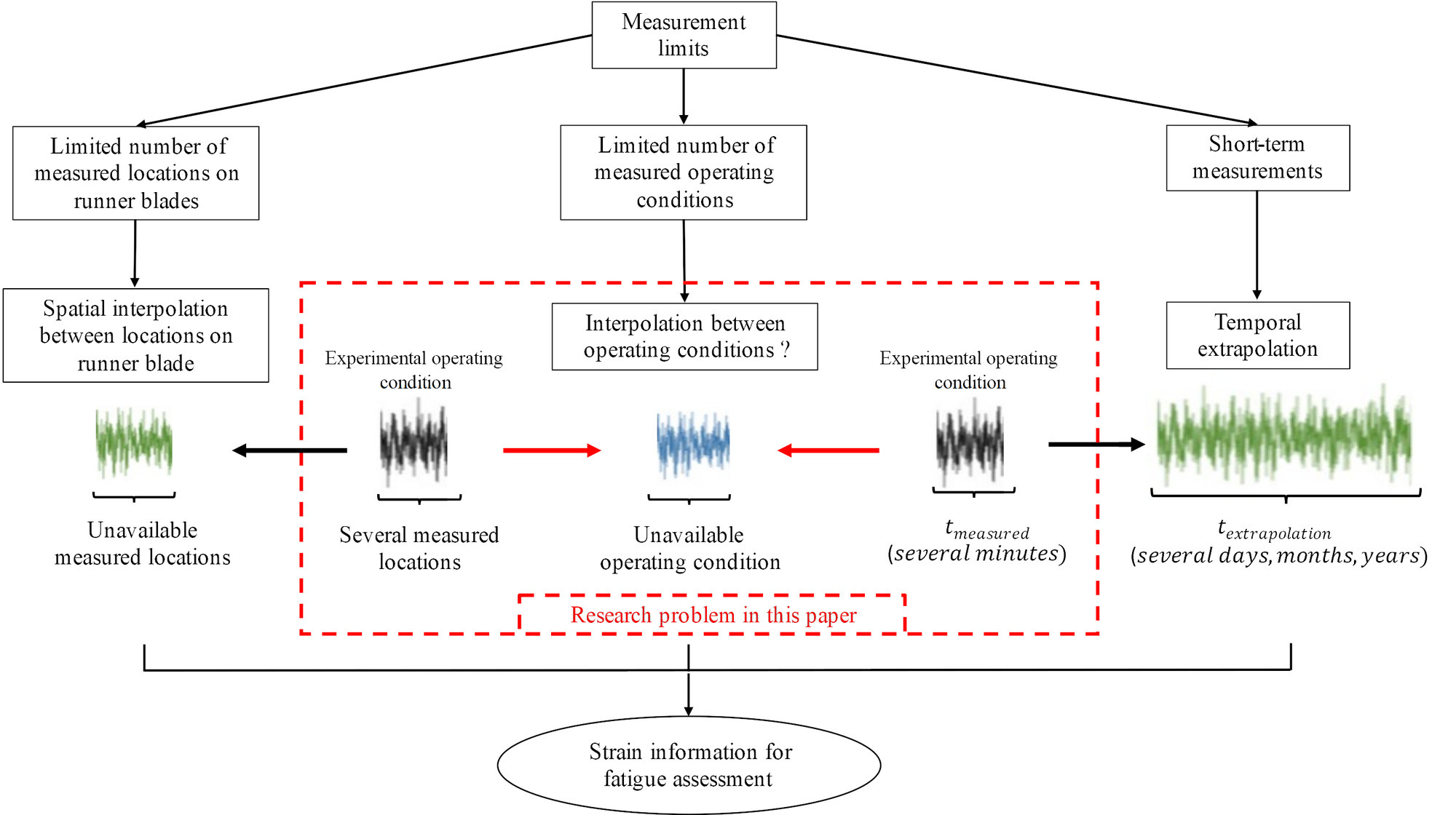
Measurement limits
Limited number of measured locations on runner blades
Limited number of measured operating conditions
Short-term measurements
Spatial interpolation between locations on runner blade
Interpolation between operating conditions ?
Temporal extrapolation
Experimental operating condition
Experimental operating condition
Unavailable measured locations
Several measured locations
Unavailable operating condition
$t_{measured}$ (several minutes)
$t_{extrapolation}$ (several days, months, years)
Research problem in this paper
Strain information for fatigue assessment

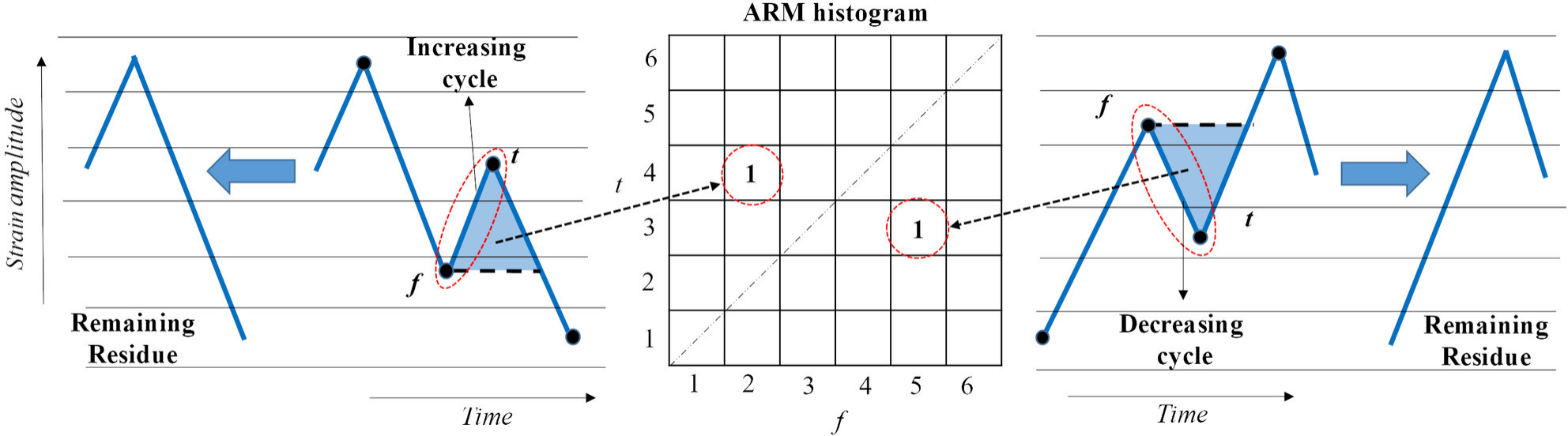
ARM histogram
Strain amplitude
Increasing cycle
t
f
Remaining Residue
Time
6
5
4
3
2
1
t
1
1
1 2 3 4 5 6
f
f
t
Decreasing cycle
Remaining Residue
Time

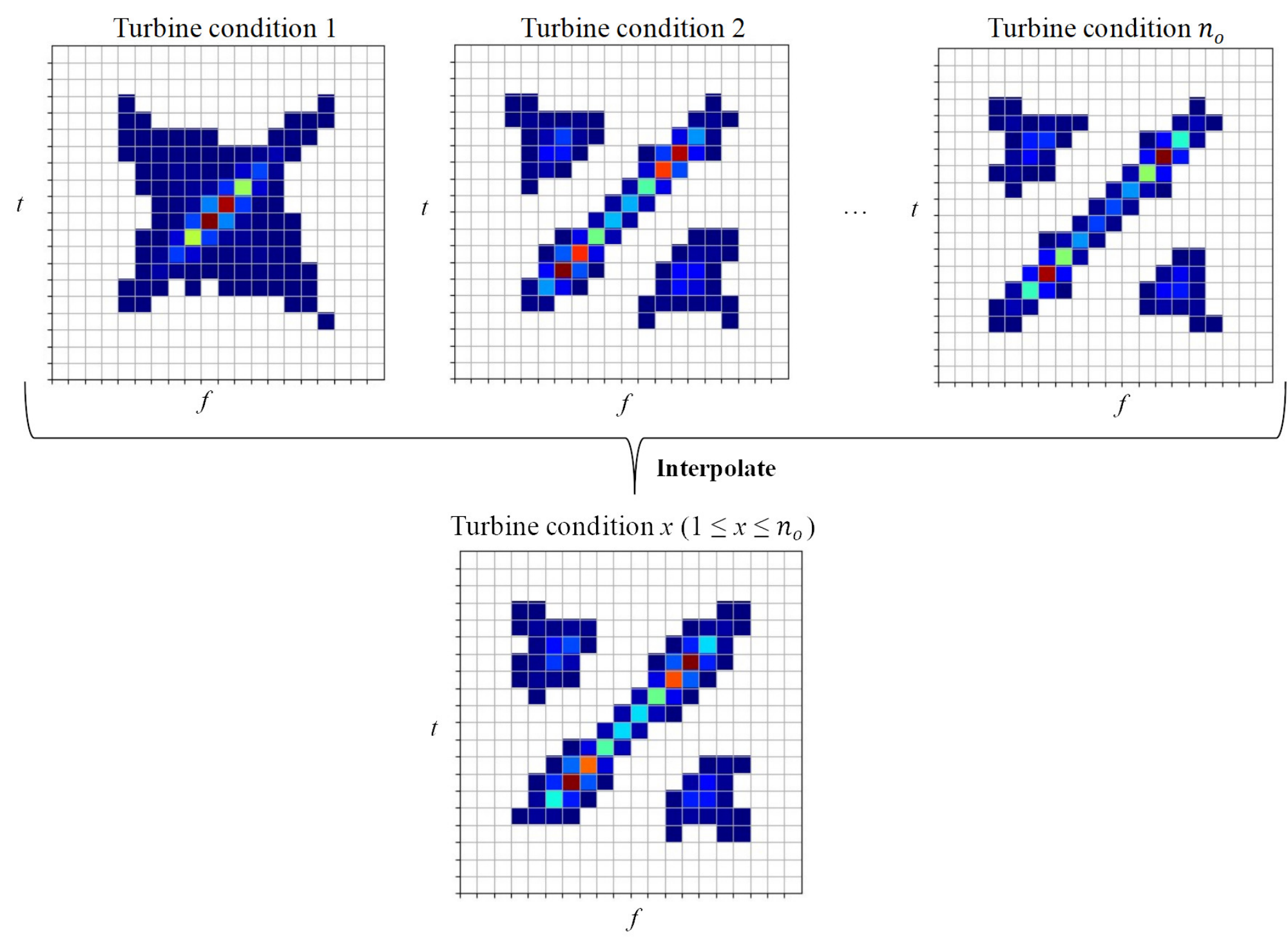
Turbine condition 1
Turbine condition 2
Turbine condition n_o
t
f
...
Interpolate
Turbine condition x ($1 \leq x \leq n_o$)

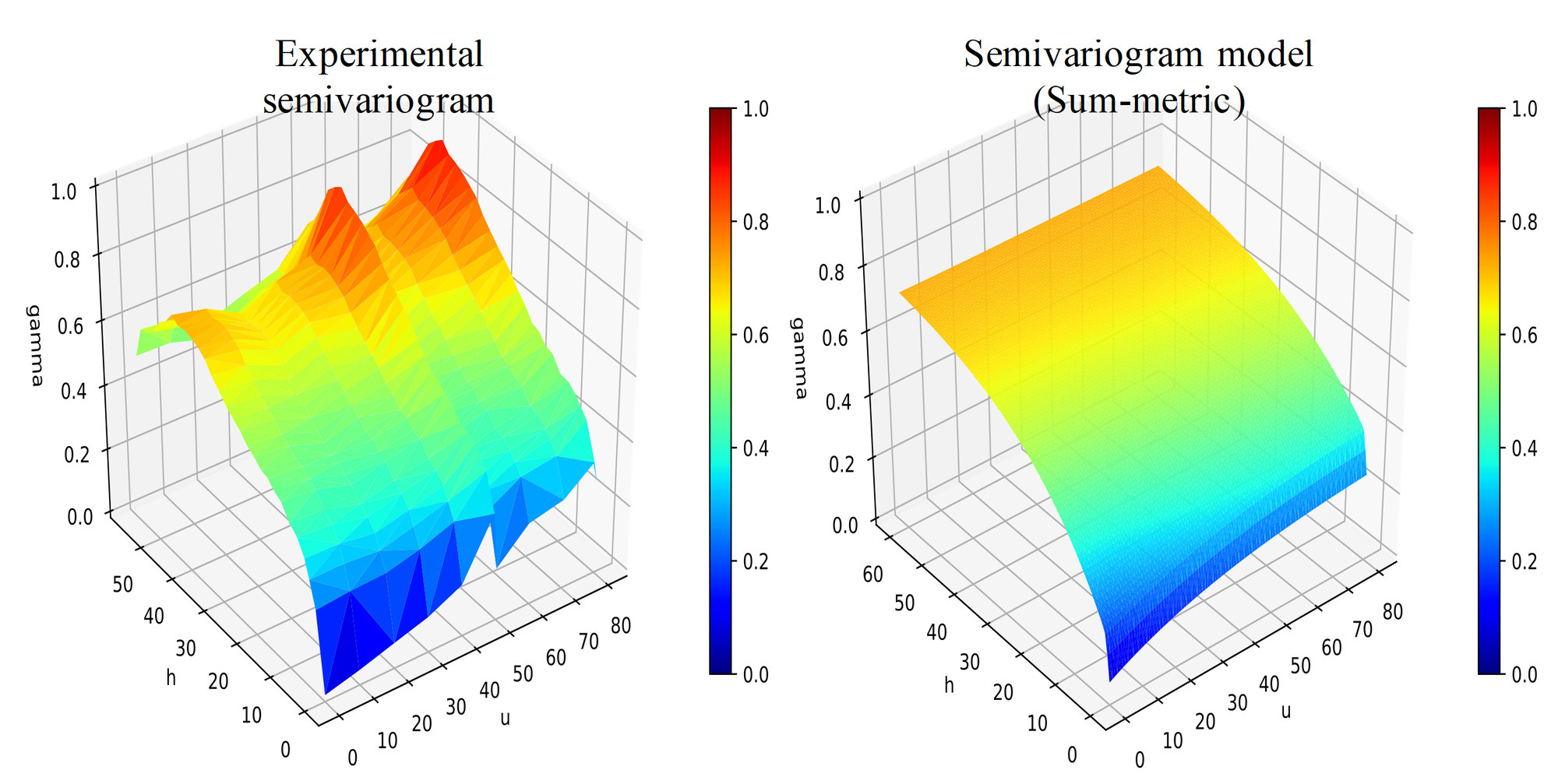
Experimental
semivariogram
gamma
1.0
0.8
0.6
0.4
0.2
0.0
h
0
10
20
30
40
50
u
0
10
20
30
40
50
60
70
80
1.0
0.8
0.6
0.4
0.2
0.0
Semivariogram model
(Sum-metric)
gamma
1.0
0.8
0.6
0.4
0.2
0.0
h
0
10
20
30
40
50
60
u
0
10
20
30
40
50
60
70
80
1.0
0.8
0.6
0.4
0.2
0.0

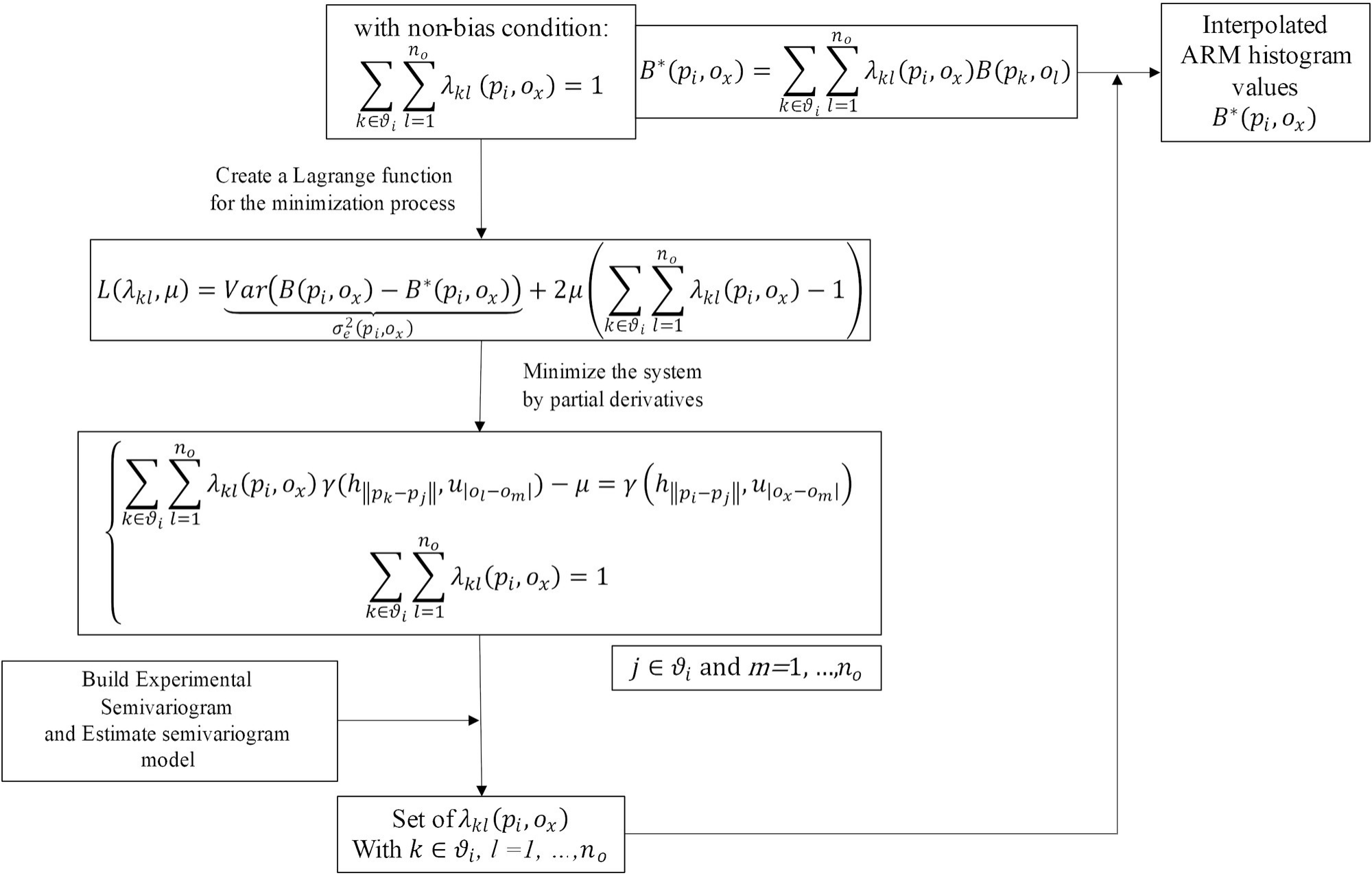
with non-bias condition:
$\sum_{k\in\vartheta_i}\sum_{l=1}^{n_o}\lambda_{kl}(p_i,o_x)=1$
$B^*(p_i,o_x)=\sum_{k\in\vartheta_i}\sum_{l=1}^{n_o}\lambda_{kl}(p_i,o_x)B(p_k,o_l)$
Interpolated ARM histogram values $B^*(p_i,o_x)$
Create a Lagrange function for the minimization process
$L(\lambda_{kl},\mu)=\underbrace{Var\left(B(p_i,o_x)-B^*(p_i,o_x)\right)}_{\sigma_e^2(p_i,o_x)}+2\mu\left(\sum_{k\in\vartheta_i}\sum_{l=1}^{n_o}\lambda_{kl}(p_i,o_x)-1\right)$
Minimize the system by partial derivatives
$\sum_{k\in\vartheta_i}\sum_{l=1}^{n_o}\lambda_{kl}(p_i,o_x)\,\gamma(h_{\|p_k-p_j\|},u_{|o_l-o_m|})-\mu=\gamma\left(h_{\|p_i-p_j\|},u_{|o_x-o_m|}\right)$
$\sum_{k\in\vartheta_i}\sum_{l=1}^{n_o}\lambda_{kl}(p_i,o_x)=1$
$j\in\vartheta_i$ and m=1, ...,n_o
Build Experimental Semivariogram and Estimate semivariogram model
Set of $\lambda_{kl}(p_i,o_x)$ With $k\in\vartheta_i$, l =1, ...,n_o

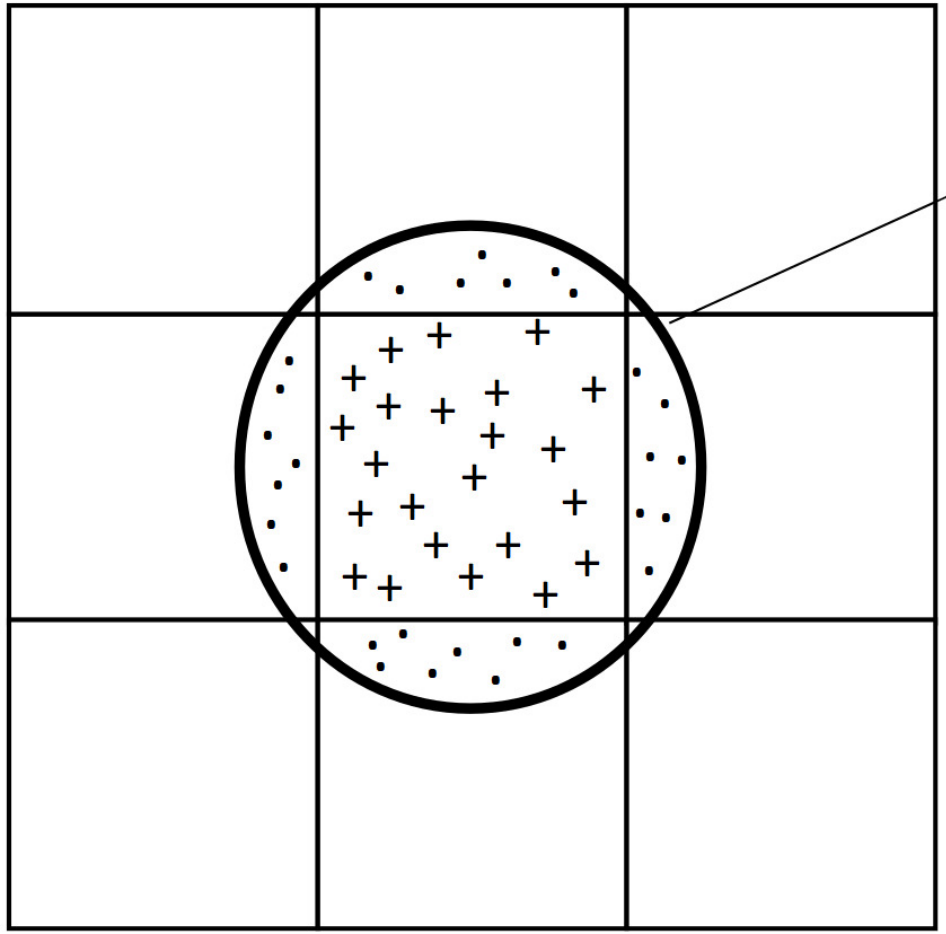

Contour of bivariate Gaussian distribution

Points inside the bin

Points outside the bin

$$\frac{\text{Points outside the bin}}{\text{Total points}} \approx y\%$$

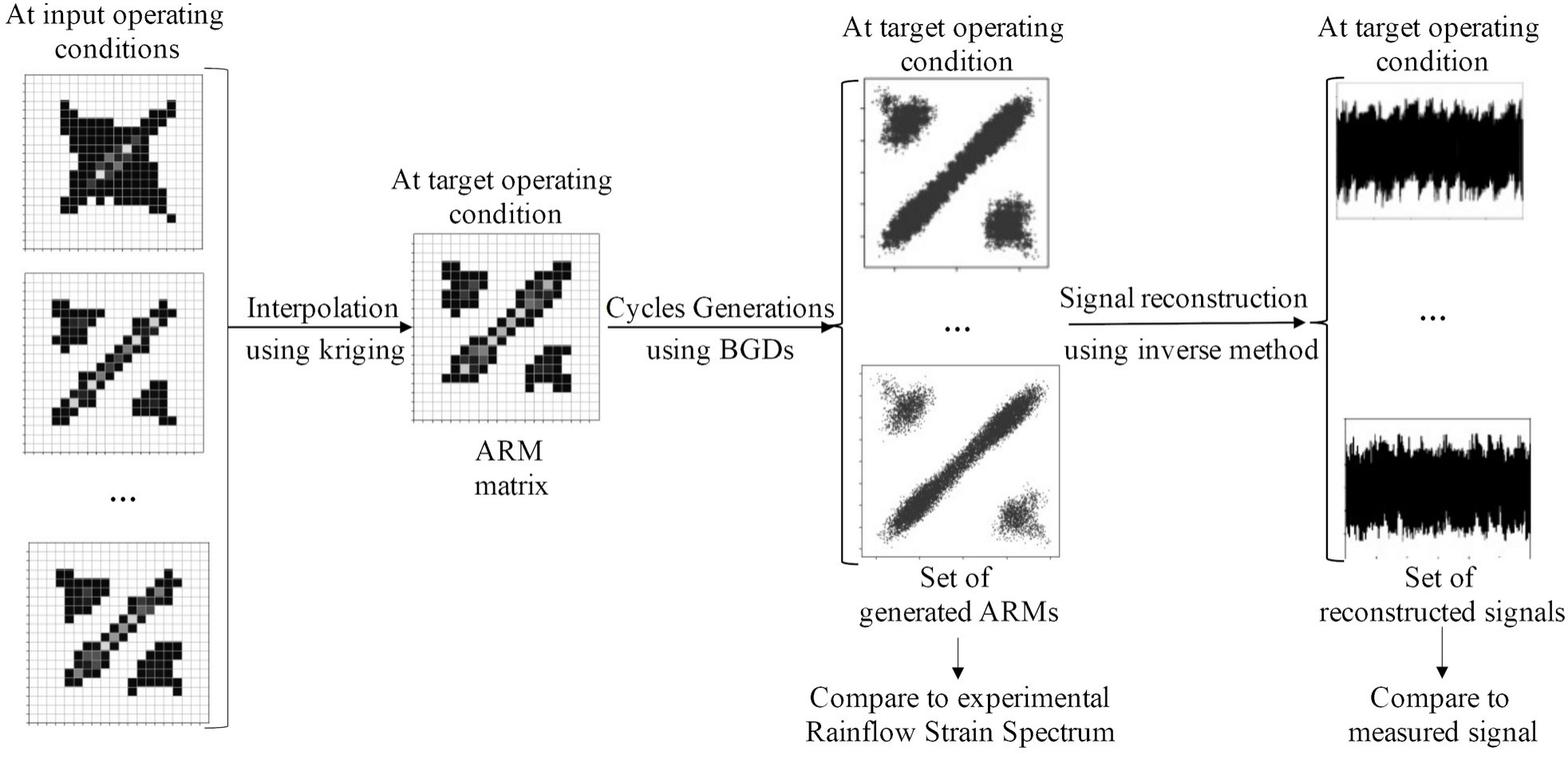
At input operating conditions
...
Interpolation using kriging
At target operating condition
ARM matrix
Cycles Generations using BGDs
At target operating condition
...
Set of generated ARMs
Compare to experimental Rainflow Strain Spectrum
Signal reconstruction using inverse method
At target operating condition
...
Set of reconstructed signals
Compare to measured signal

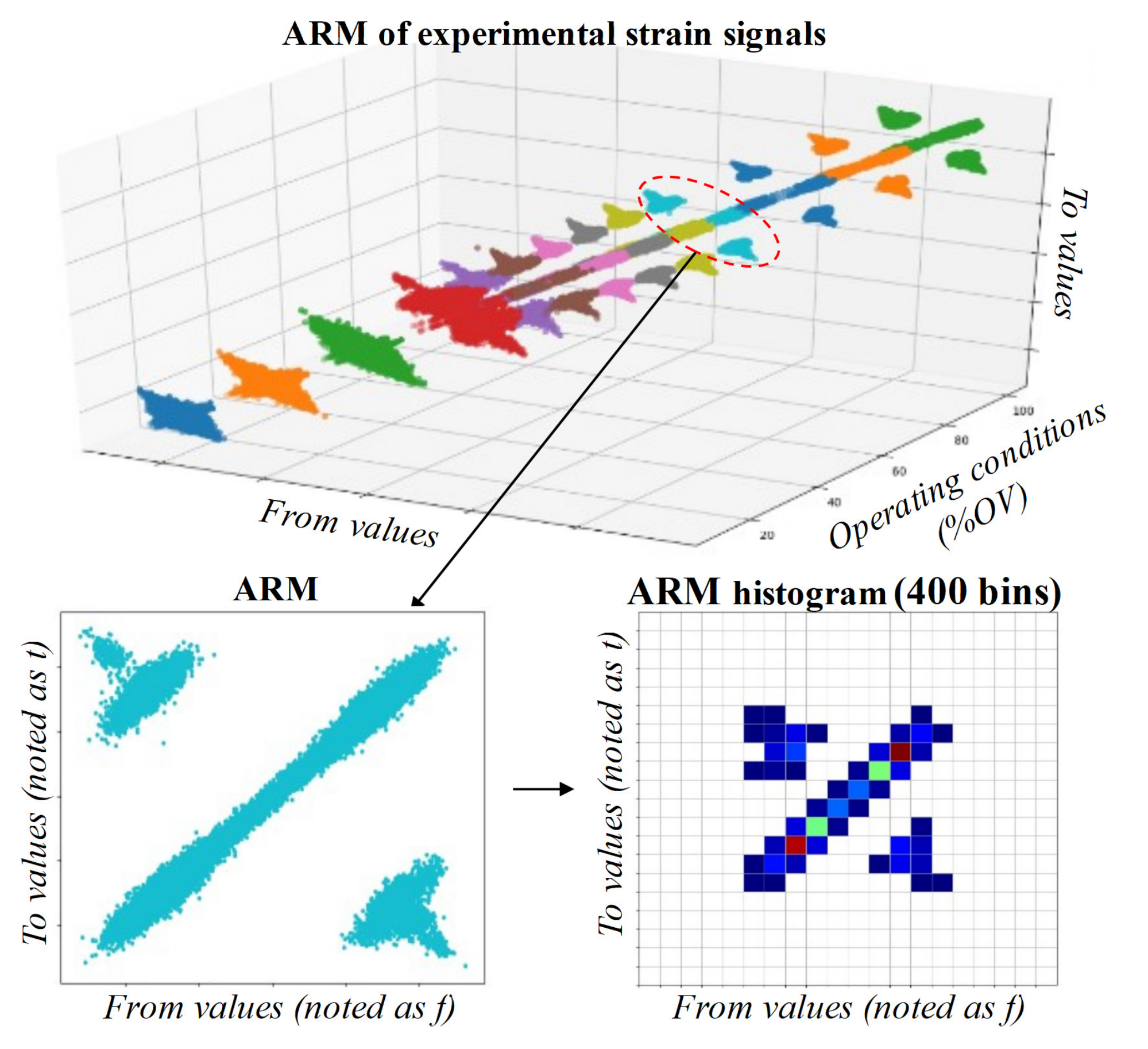
ARM of experimental strain signals
To values
From values
Operating conditions (%OV)
20
40
60
80
100
ARM
To values (noted as t)
From values (noted as f)
ARM histogram (400 bins)
To values (noted as t)
From values (noted as f)

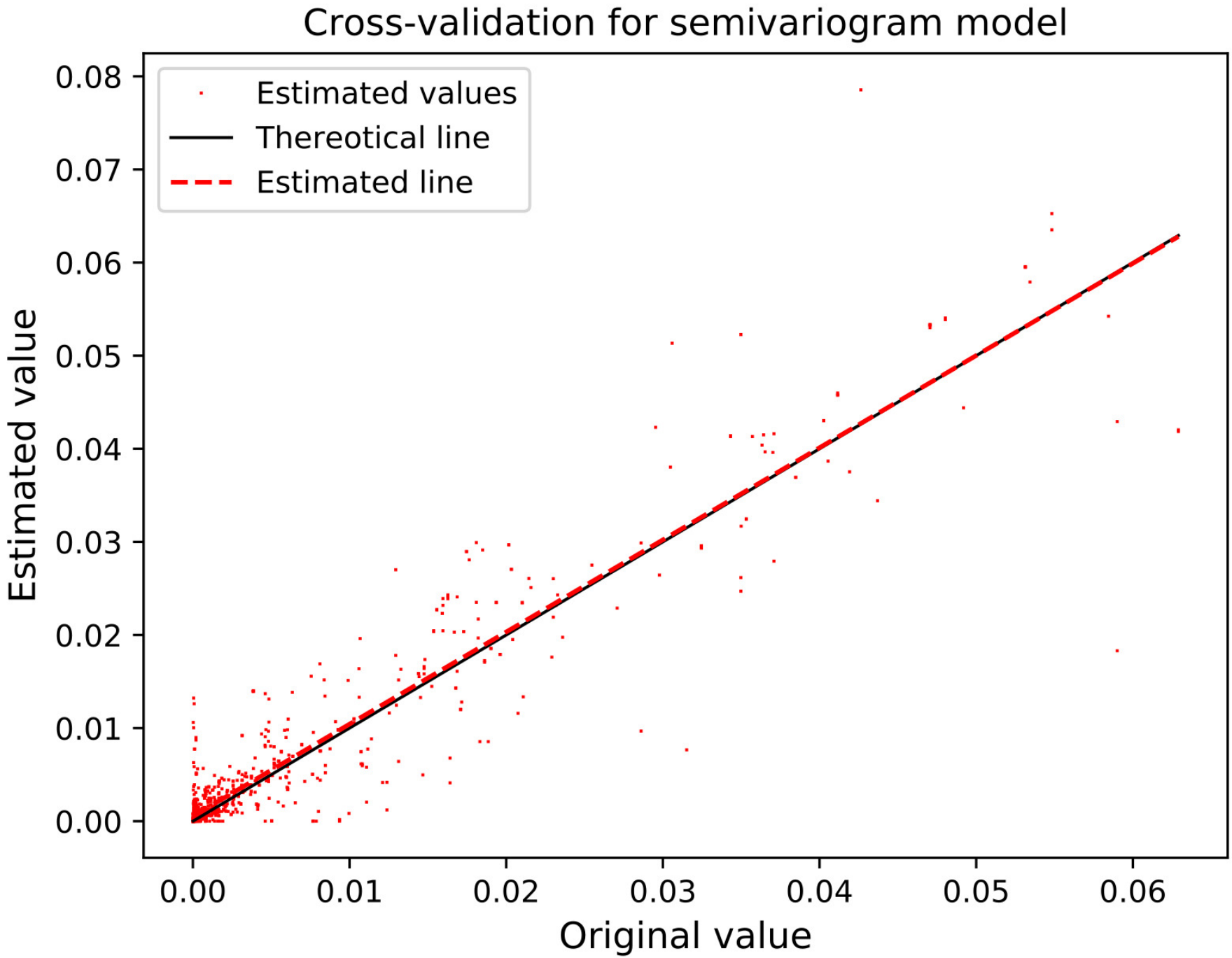
Cross-validation for semivariogram model
Estimated values
Thereotical line
Estimated line
Estimated value
Original value
0.00
0.01
0.02
0.03
0.04
0.05
0.06
0.07
0.08

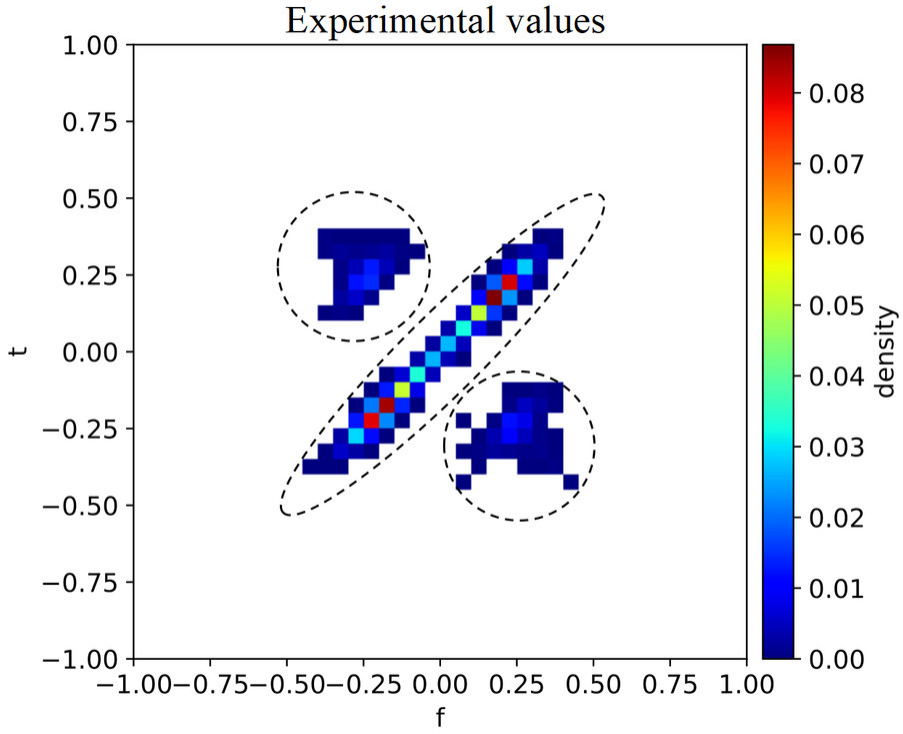
Experimental values
1.00
0.75
0.50
0.25
0.00
−0.25
−0.50
−0.75
−1.00
t
−1.00 −0.75 −0.50 −0.25 0.00 0.25 0.50 0.75 1.00
f
0.08
0.07
0.06
0.05
0.04
0.03
0.02
0.01
0.00
density

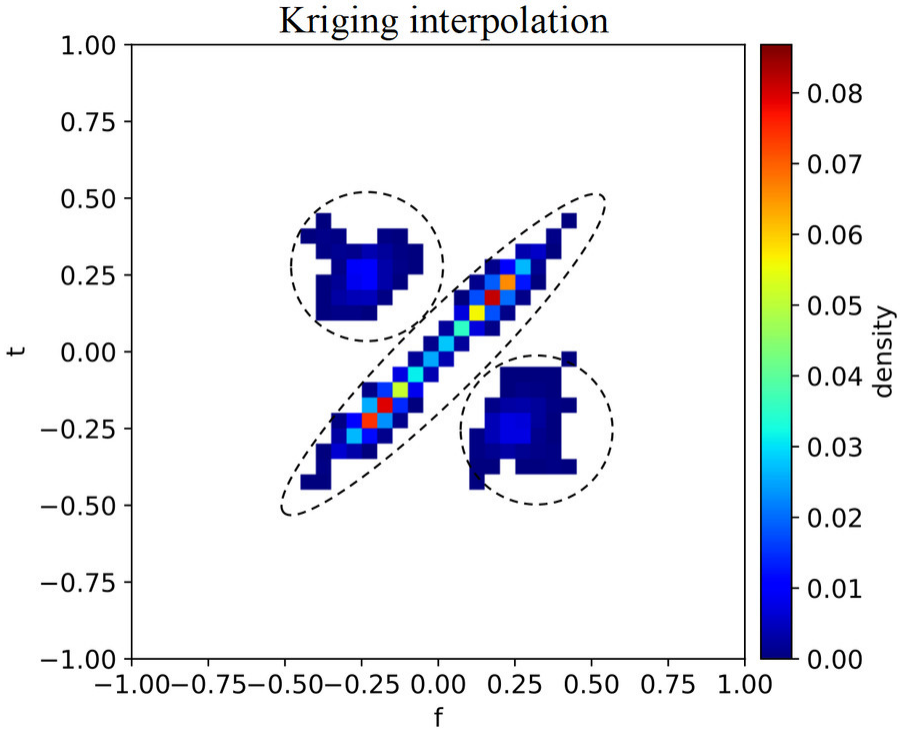
Kriging interpolation
1.00
0.75
0.50
0.25
0.00
−0.25
−0.50
−0.75
−1.00
t
−1.00 −0.75 −0.50 −0.25 0.00 0.25 0.50 0.75 1.00
f
0.08
0.07
0.06
0.05
0.04
0.03
0.02
0.01
0.00
density

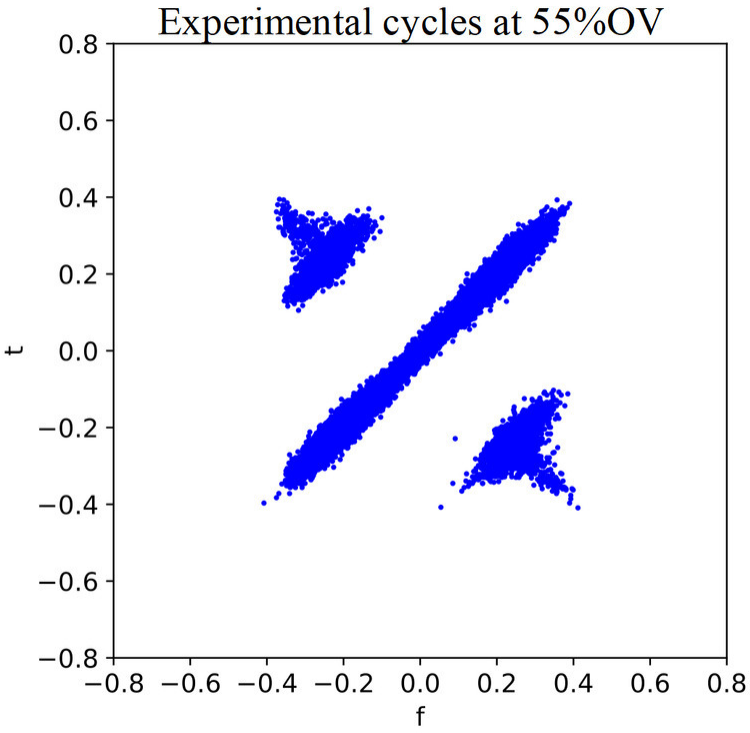
Experimental cycles at 55%OV
0.8
0.6
0.4
0.2
0.0
−0.2
−0.4
−0.6
−0.8
t
−0.8 −0.6 −0.4 −0.2 0.0 0.2 0.4 0.6 0.8
f

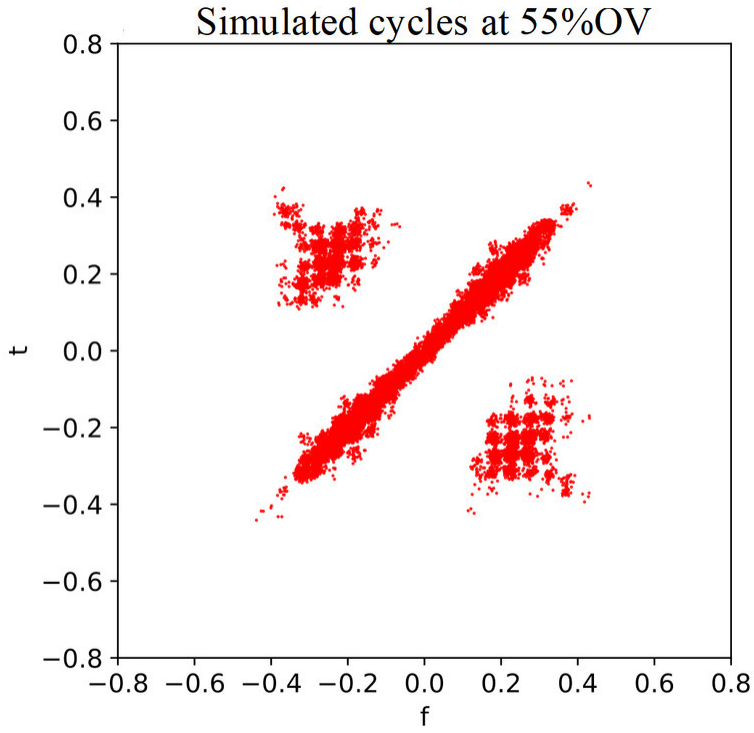
Simulated cycles at 55%OV
0.8
0.6
0.4
0.2
0.0
−0.2
−0.4
−0.6
−0.8
t
−0.8 −0.6 −0.4 −0.2 0.0 0.2 0.4 0.6 0.8
f

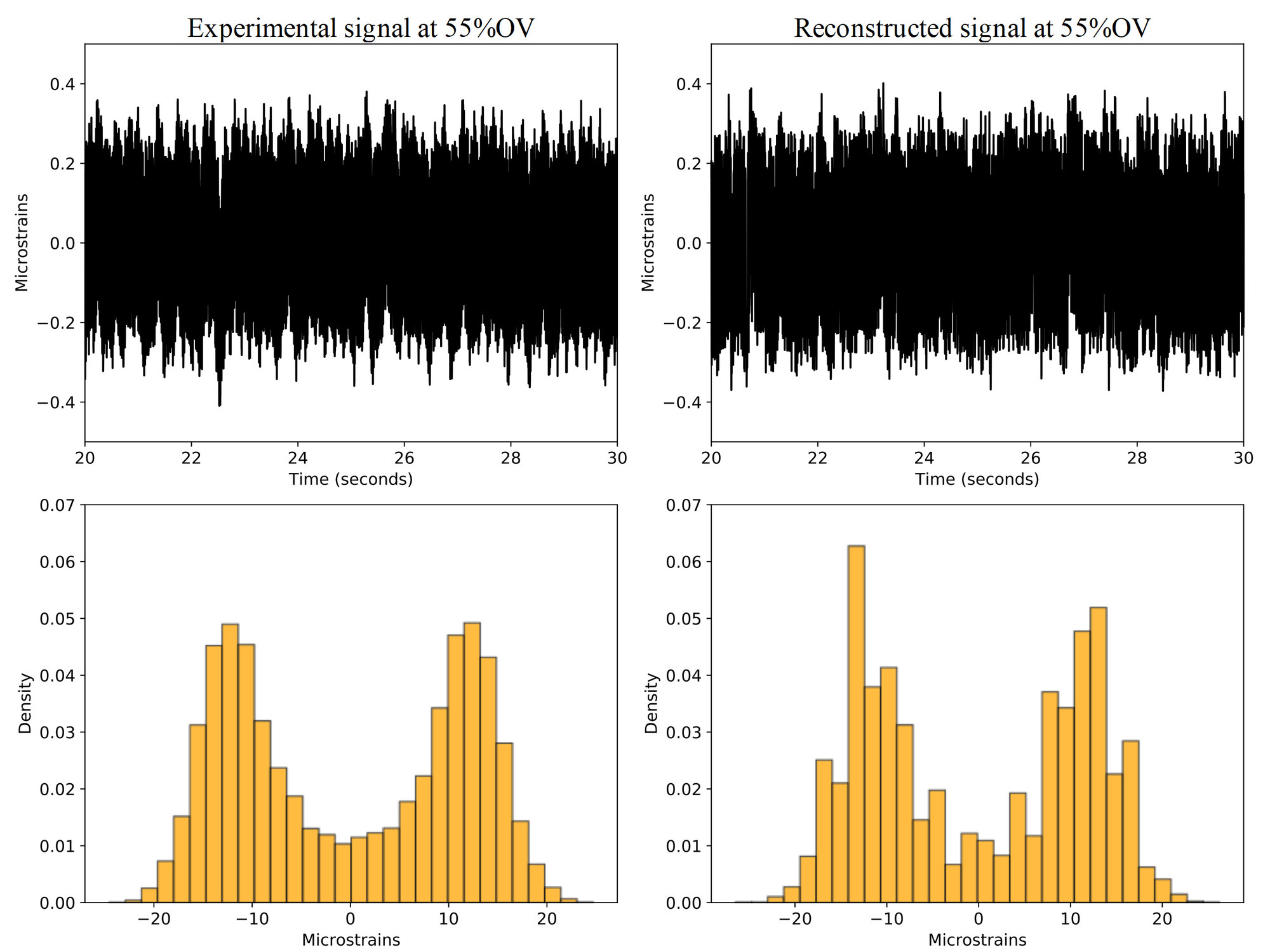
Experimental signal at 55%OV
Reconstructed signal at 55%OV
Microstrains
Time (seconds)
Density
Microstrains
0.4
0.2
0.0
−0.2
−0.4
20
22
24
26
28
30
0.07
0.06
0.05
0.04
0.03
0.02
0.01
0.00
−20
−10
0
10
20

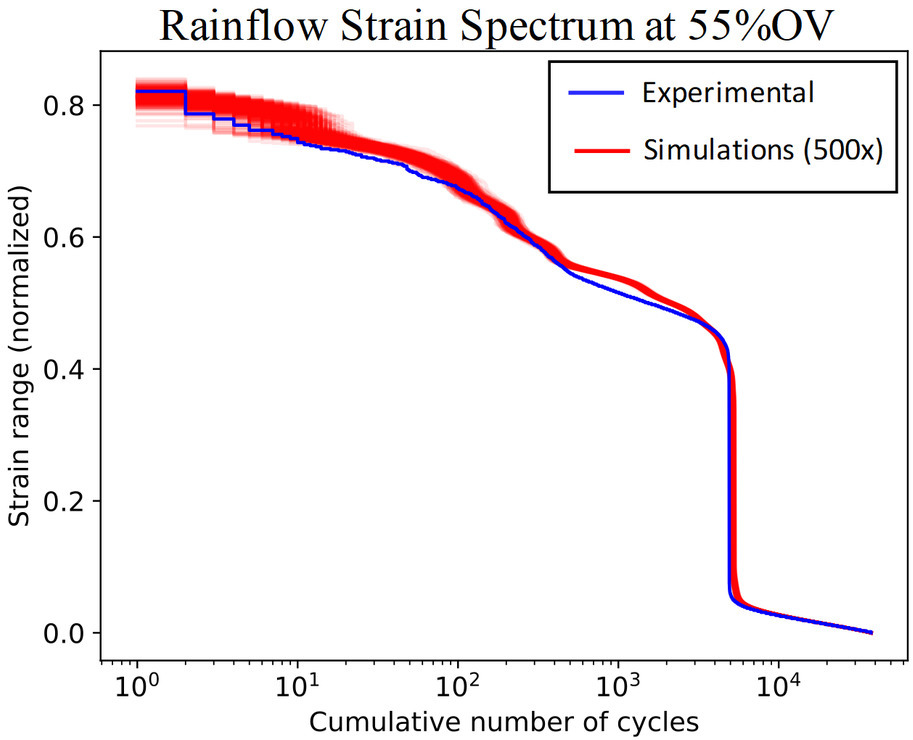
Rainflow Strain Spectrum at 55%OV
Experimental
Simulations (500x)
Strain range (normalized)
Cumulative number of cycles

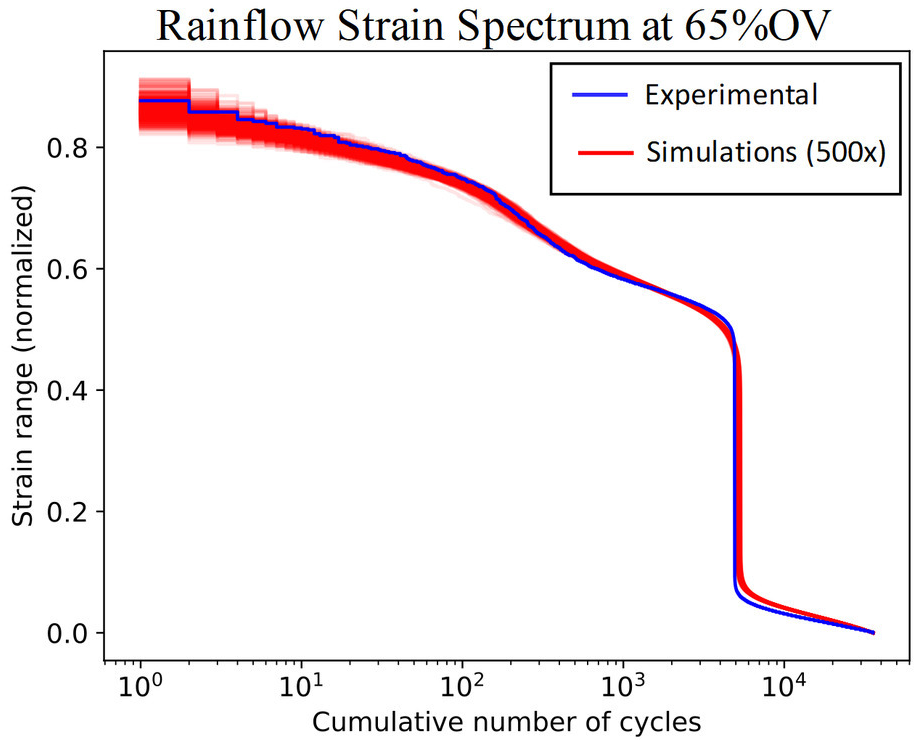
Rainflow Strain Spectrum at 65%OV
Experimental
Simulations (500x)
Strain range (normalized)
Cumulative number of cycles

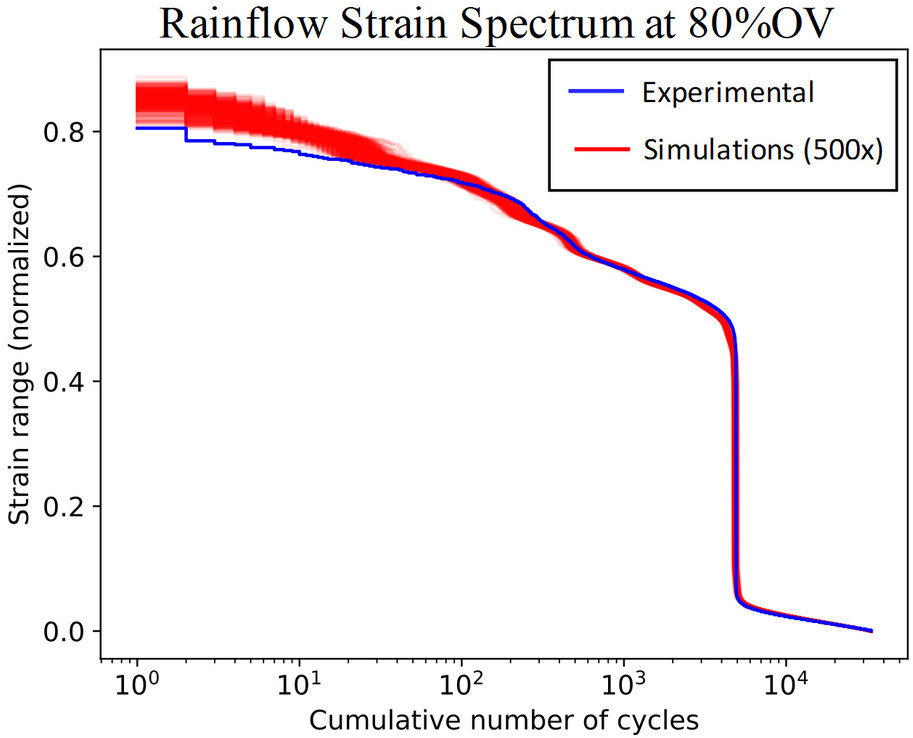
Rainflow Strain Spectrum at 80%OV
Experimental
Simulations (500x)
Strain range (normalized)
Cumulative number of cycles

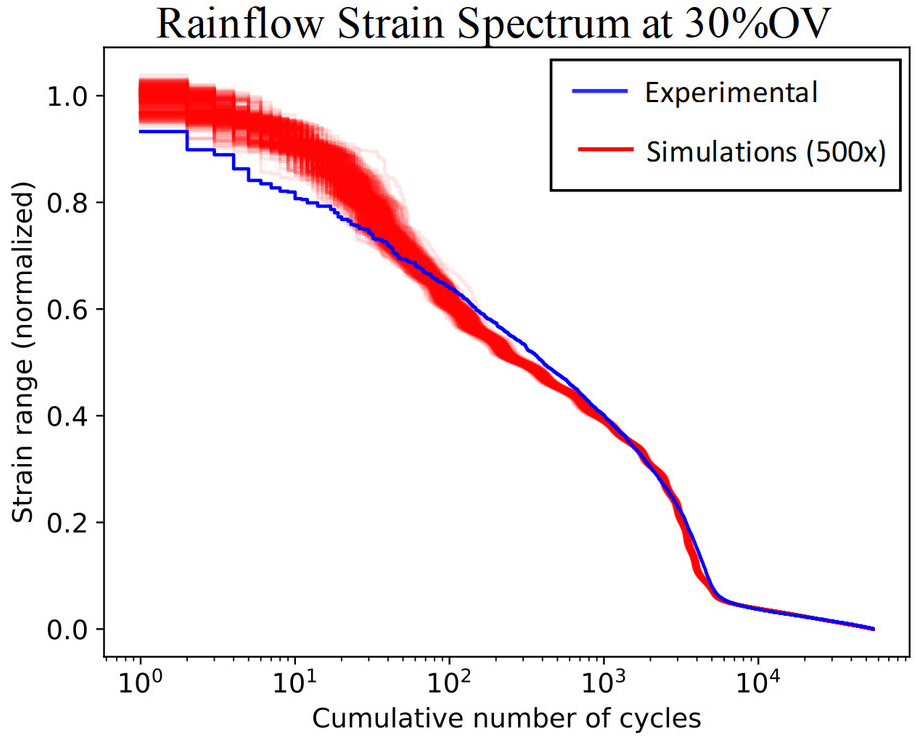
Rainflow Strain Spectrum at 30%OV
Experimental
Simulations (500x)
Strain range (normalized)
Cumulative number of cycles

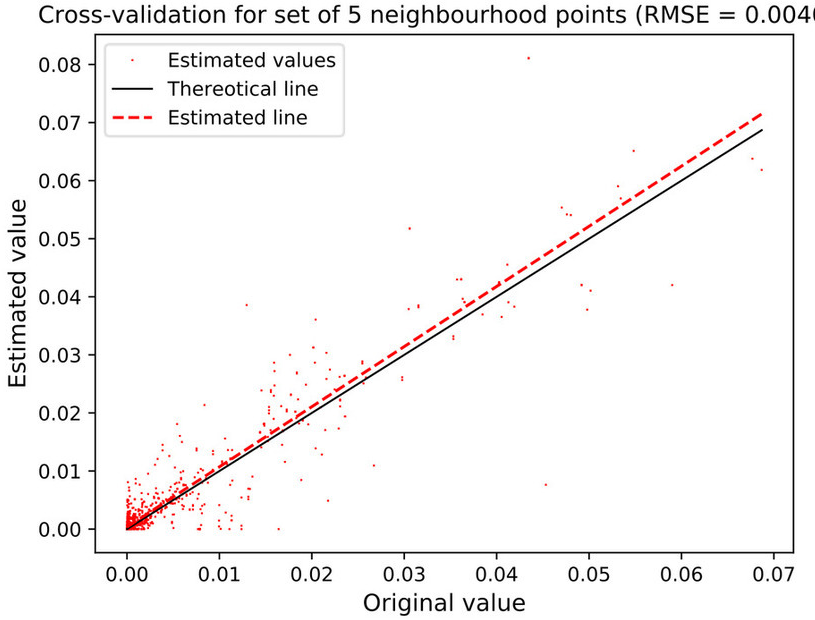
Cross-validation for set of 5 neighbourhood points (RMSE = 0.00404)
Estimated values
Thereotical line
Estimated line
Estimated value
Original value

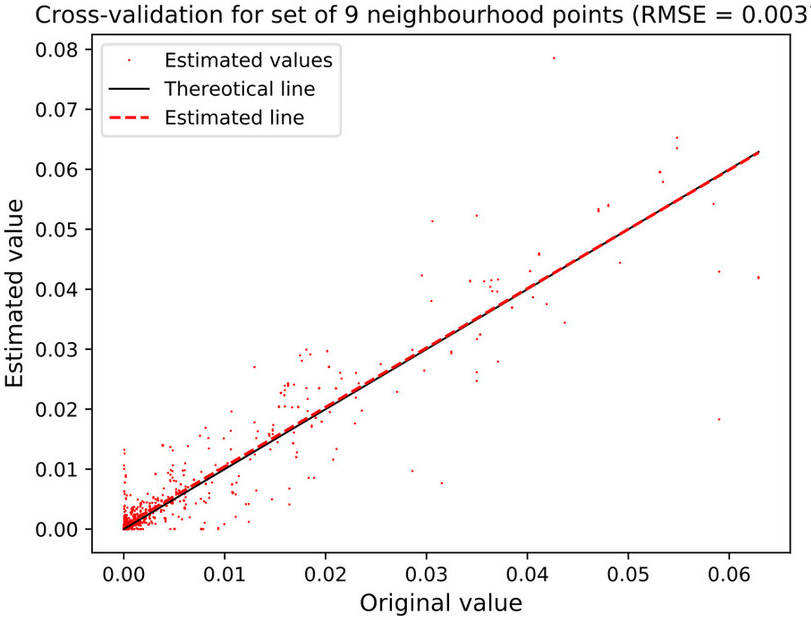
Cross-validation for set of 9 neighbourhood points (RMSE = 0.00379)
Estimated values
Thereotical line
Estimated line
Estimated value
Original value

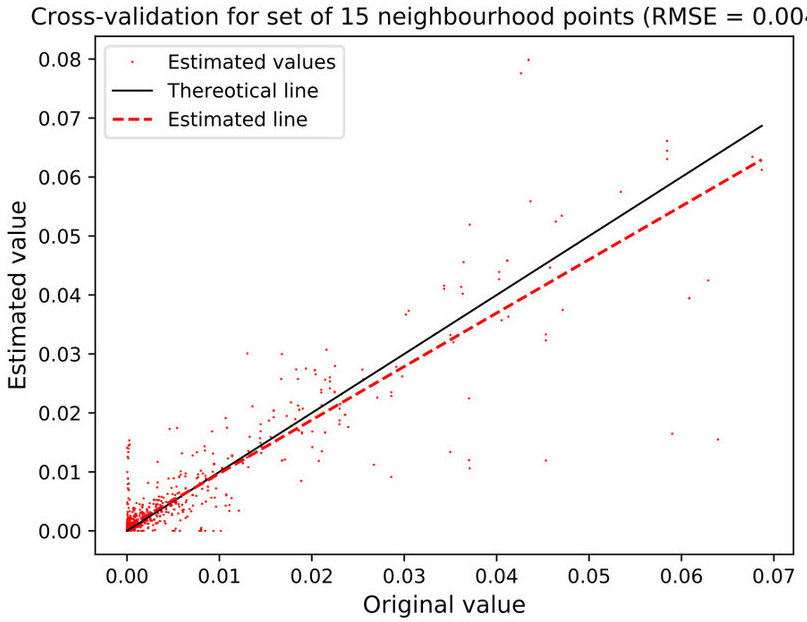
Cross-validation for set of 15 neighbourhood points (RMSE = 0.00466)
Estimated values
Thereotical line
Estimated line
Estimated value
Original value

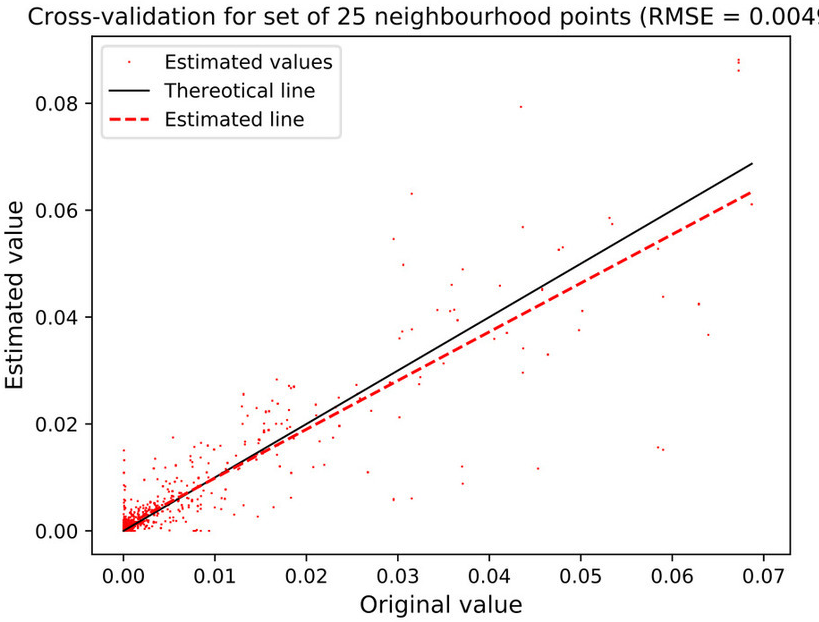
Cross-validation for set of 25 neighbourhood points (RMSE = 0.00495)
Estimated values
Thereotical line
Estimated line
Estimated value
Original value

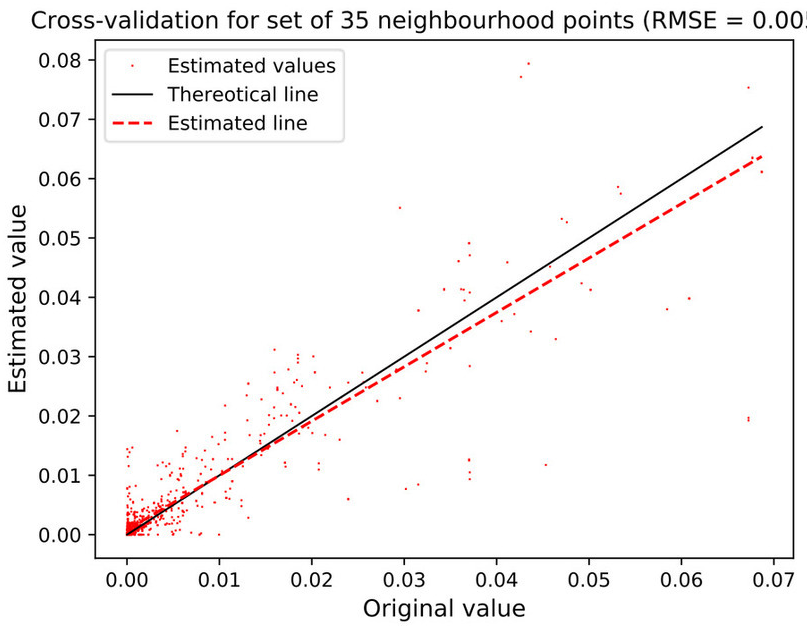
Cross-validation for set of 35 neighbourhood points (RMSE = 0.00515)
Estimated values
Thereotical line
Estimated line
Estimated value
Original value

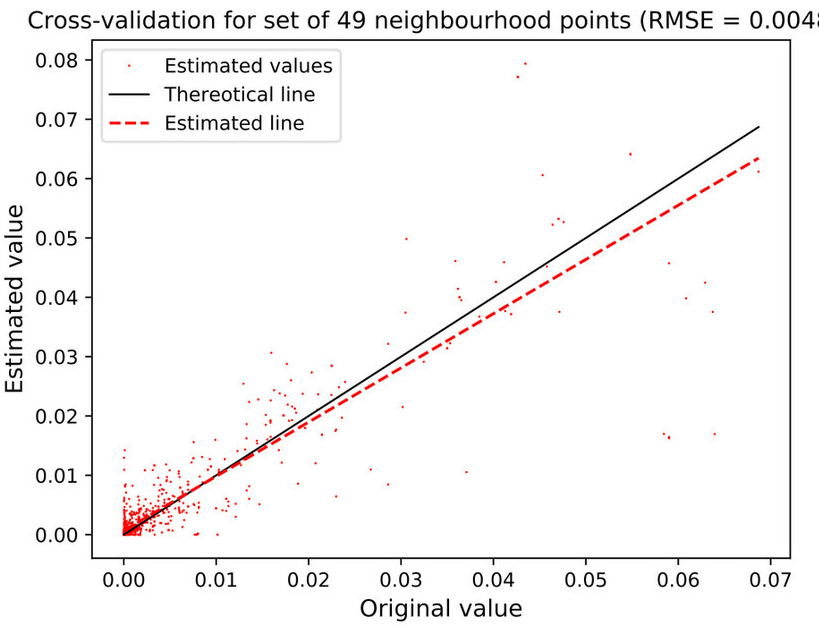
Cross-validation for set of 49 neighbourhood points (RMSE = 0.00481)
Estimated values
Thereotical line
Estimated line
Estimated value
Original value